



OPEN

# A new nanomagnetic Pd-Co bimetallic alloy as catalyst in the Mizoroki–Heck and Buchwald–Hartwig amination reactions in aqueous media

Sara Sobhani<sup>1</sup>✉, Hamed Zarei<sup>1</sup> & José Miguel Sansano<sup>2</sup>

A Pd-Co bimetallic alloy encapsulated in melamine-based dendrimer supported on magnetic nanoparticles denoted as  $\gamma\text{-Fe}_2\text{O}_3\text{@MBD/Pd-Co}$  was synthesized by a facile co-complexation-reduction method and characterized sufficiently. The catalytic evaluation of  $\gamma\text{-Fe}_2\text{O}_3\text{@MBD/Pd-Co}$  showed promising results in the Mizoroki–Heck and Buchwald–Hartwig amination reactions of various iodo-, bromo- and challenging chloroarenes in aqueous media. The synergetic cooperative effect of both Pd and Co and dispersion of the catalyst in water due to the encapsulation of  $\gamma\text{-Fe}_2\text{O}_3$  by melamine-based dendrimer lead to high catalytic performance compared with the monometallic counterparts. The dispersion of the magnetic catalyst also facilitates the recovery and reuse of the catalyst by ten consecutive extraction and final magnetic isolation with no loss of catalytic activity, keeping its structure unaltered.

Haloarenes are frequently transformed into a variety of valuable compounds catalyzed by transition metals such as palladium, copper, nickel, and cobalt with various ligands through cross-coupling reactions<sup>1–4</sup>. Concerning the catalytic metals employed, palladium is the most versatile element in industrial and academic research playing the most prominent part in the removal of halogen atom from halogenated organic compounds. Therefore, since the pioneering works, the homogeneous palladium complexes have attracted the interest of scientists to address coupling reactions due to their excellent functional group tolerance, as well as their excellent catalytic efficiency<sup>5</sup>. However, application of homogeneous palladium catalysts has some limitations such as non-reusability, high cost, poisoning and losing activity, which are important from economic and environmental viewpoints. These problems can be largely overcome by supporting Pd nanoparticles (NPs) or complexes on varied solid supports<sup>6</sup>. Moreover, considering the consumption of expensive Pd, the development of bimetallic nanoparticles of non-noble metal elements with Pd can not only reduce costs, but also stabilizes active Pd species, and improves its resistance to poisoning<sup>7</sup>. The supported bimetallic nanoparticles with two special advantages of using of a lower quantity of Pd and the recovery of the heterogeneous NPs by filtration from the reaction media, could be used as suitable catalysts in cross-coupling reactions. Moreover, because of the synergistic effect, the catalytic activity and selectivity obtained over bimetallic nanoparticles were much higher than that obtained over the monometallic counterparts. Along this line, Pd-based bimetallic nanoparticles including Pd–Ag, Pd–Cu, Pd–Co, Pd–Au or Pd–Ni, supported on different solid substances have been reported<sup>7–11</sup>. Although heterogeneous catalysts can be recovered by filtration or centrifugation methods, these methods are time consuming, and result the impurities in the product due to the loss of the catalyst particles.

In recent decades, magnetic nanoparticles (MNPs), which have been widely surveyed towards many medical and biological uses, have emerged as modern and attractive materials for the supporting of catalytically active species. The magnetically immobilized catalysts can be isolated from the reaction mixture employing magnets<sup>12,13</sup>. This separation is operationally very simple, economic and promising for industrial applications. Moreover, MNPs possess exclusive physical properties, for example, high surface area, surface modification ability and extraordinary thermal and chemical stabilities. However, MNPs suffer from aggregation during the catalytic

<sup>1</sup>Department of Chemistry, College of Sciences, University of Birjand, Birjand, Iran. <sup>2</sup>Departamento de Química Orgánica, Facultad de Ciencias, Centro de Innovación en Química Avanzada (ORFEO-CINQA) and Instituto de Síntesis Orgánica (ISO), Universidad de Alicante, Apdo. 99, 03080 Alicante, Spain. ✉email: ssobhani@birjand.ac.ir

processes, resulting in a sensible decrease in their catalytic efficiency. Therefore, encapsulation of MNPs using noble metals, carbon, silica and biopolymers stabilize and protect them from oxidation and agglomeration<sup>14,15</sup>.

Dendrimers are a relatively novel class of polymers with a well-defined highly branched, three-dimensional structure and are being used for encapsulation of MNPs<sup>16</sup>. In the dendrimers, the existence of several inner and outer functional groups allows the coordination with transition metals contributing to their stabilization. Because of this property, dendrimers are principally suitable host for metal catalysts. Nanometals are encapsulated within the dendrimer cavities, so that their agglomeration is circumvented and the well-dispersed nanoparticles are obtained. Moreover, the existence of a large number of cavities in dendritic polymers, could absorb and concentrate reactants, and makes the reaction proceed more efficiently. Importantly, the substrates can still simply contact with the encapsulated catalytically active nanoparticle in the dendrimers. As the melamine is rich with nitrogen and contains triazine rings with high stability, melamine-based dendrimers (MBD) with abundant metal-binding nitrogen groups have aroused a lot of interest recently for the incorporation of metal nanoparticles for using in catalytic reactions<sup>17–19</sup>.

In our continuous interest in developing a greener catalyzed reaction<sup>4,20–28</sup>, herein, a melamine-based dendrimer was built to the 1.5-generation onto the  $\gamma$ -Fe<sub>2</sub>O<sub>3</sub> surface employing a divergent method to synthesize  $\gamma$ -Fe<sub>2</sub>O<sub>3</sub>@melamine-based dendrimer ( $\gamma$ -Fe<sub>2</sub>O<sub>3</sub>@MBD). Bimetallic Pd-Co alloy nanoparticles were then attached to  $\gamma$ -Fe<sub>2</sub>O<sub>3</sub>@melamine-based dendrimer via a co-complexation method followed by reduction with sodium borohydride. This novel catalyst was fully analyzed by several instrumental techniques and applied as a water-dispersible/magnetically reusable palladium-cobalt catalyst for the Mizoroki–Heck and Buchwald–Hartwig amination reactions in aqueous media. The synergistic cooperative effect of both Pd and Co in the catalyst lead to high catalytic performance in the cross-coupling reactions in aqueous media.

## Experimental section

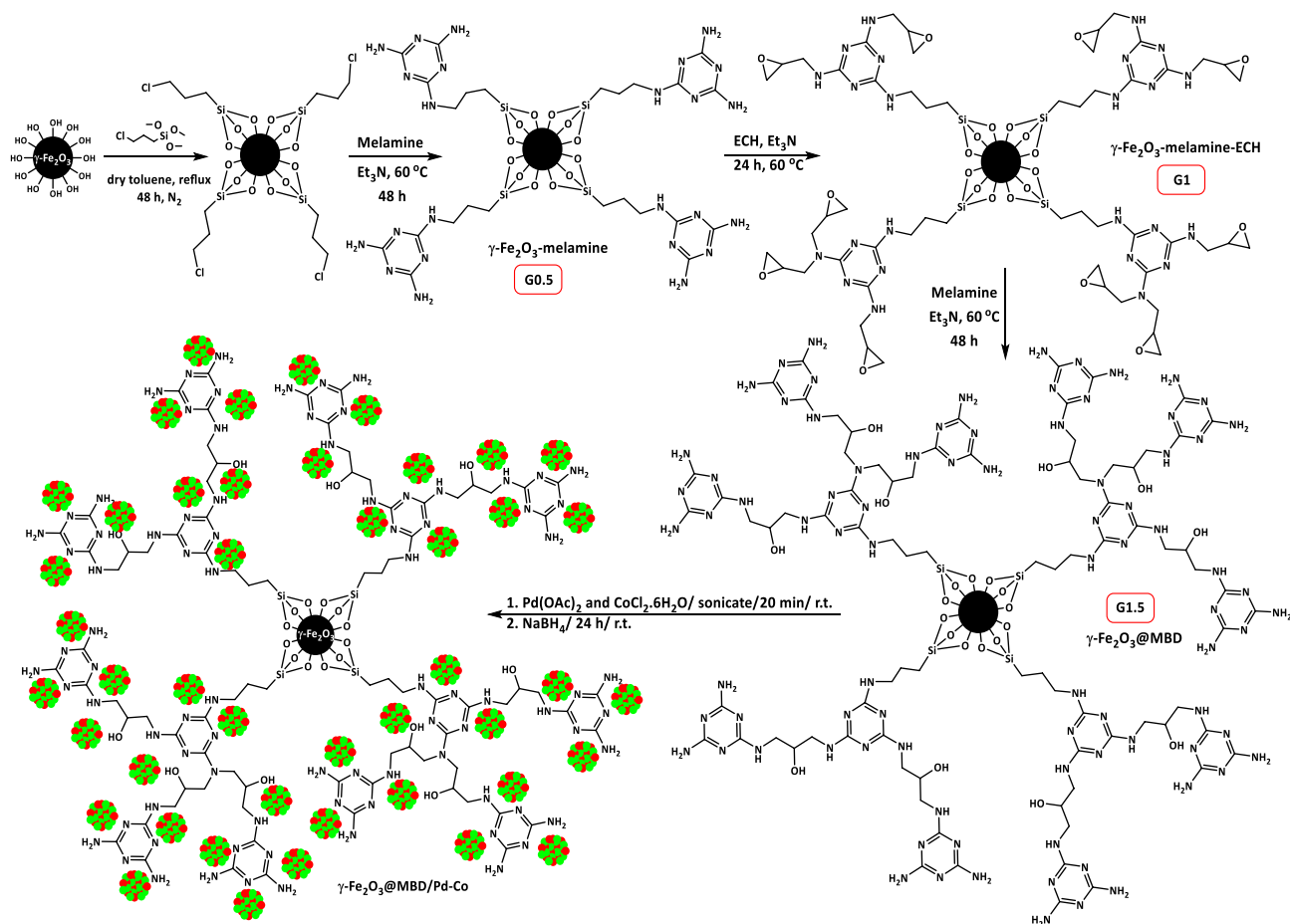
**Materials and methods.** Chemicals were purchased from Merck Chemical Company. NMR spectra were recorded on a Bruker Avance DPX-400 and 300 using deuterated CDCl<sub>3</sub> and DMSO-d<sub>6</sub> as solvent and TMS as internal standard. The purity of the products and the progress of the reactions were accomplished by TLC on silica-gel polygram SILG/UV254 plates. TEM analysis was performed using TEM microscope (Philips EM 208S). EDS mapping were found using a TSCAN MIRA3. FT-IR spectra were recorded on a Shimadzu Fourier Transform Infrared Spectrophotometer (FT-IR-8300). Thermal gravimetric analysis (TGA) was performed using a Shimadzu thermos-gravimetric analyzer (TG-50). X-ray diffraction (XRD) was done on a Bruker D8-advance X-ray diffractometer with Cu K $\alpha$  ( $\lambda$  = 0.154 nm) radiation. XPS analyses were performed using a VG-Microtech Multilab 3000 spectrometer, equipped with an Al anode. The deconvolution of spectra was carried out by using Gaussian–Lorentzian curves. The Pd and Co content on the catalyst was determined by OPTIMA 7300DV ICP analyzer. Qualitative elemental analysis was determined and analyzed by CHNO elemental analyzer (Thermo Finnigan, FLASH EA 1112 series, Italy).

**Synthesis of  $\gamma$ -Fe<sub>2</sub>O<sub>3</sub>-melamine.** Chloro-functionalized  $\gamma$ -Fe<sub>2</sub>O<sub>3</sub><sup>20</sup> (1.5 g) was sonicated with Et<sub>3</sub>N (10 mL) and melamine (1.5 mmol, 0.18 g) for 30 min. The mixture was refluxed for 48 h at 60 °C. The resulting light-brown solid was isolated by an external magnet and washed several times with distilled H<sub>2</sub>O (3 × 20 mL) and EtOH (3 × 20 mL). It was dried in a vacuum oven at 50 °C. Elemental analysis of  $\gamma$ -Fe<sub>2</sub>O<sub>3</sub>-melamine for nitrogen (9.88%) showed that 1.2 mmol of melamine was loaded on 1 g of  $\gamma$ -Fe<sub>2</sub>O<sub>3</sub>-melamine.

**Synthesis of  $\gamma$ -Fe<sub>2</sub>O<sub>3</sub>-MBD.** The synthesized  $\gamma$ -Fe<sub>2</sub>O<sub>3</sub>-melamine from the previous step (1 g) and Et<sub>3</sub>N (10 mL) was sonicated about 30 min at room temperature. ECH (1 mL) was added to this stirring mixture drop wise. The mixture was heated to a temperature of 60 °C and kept for 24 h. Then, melamine (5 mmol, 0.63 g) was added and further stirred for 48 h at the same temperature. The resulting solid was isolated by an external magnet and washed several times with distilled H<sub>2</sub>O (3 × 20 mL) and EtOH (3 × 20 mL). It was dried in a vacuum oven at 50 °C. Elemental analysis of  $\gamma$ -Fe<sub>2</sub>O<sub>3</sub>-MBD for nitrogen (17.5%) showed that in total, 2 mmol of melamine was loaded on 1 g of  $\gamma$ -Fe<sub>2</sub>O<sub>3</sub>-MBD.

**Synthesis of  $\gamma$ -Fe<sub>2</sub>O<sub>3</sub>-MBD/Pd-Co.** A mixture of palladium acetate (0.1 g in 3.0 mL H<sub>2</sub>O) and  $\gamma$ -Fe<sub>2</sub>O<sub>3</sub>-MBD (0.2 g in 10.0 mL) sonicated for 20 min. A solution of CoCl<sub>2</sub>·6H<sub>2</sub>O (0.741, 0.529, 0.105 g in 3.0 mL H<sub>2</sub>O) was added to the resulting mixture and sonicated for further 20 min. The pH of the sonicated mixture was controlled between 8 and 10 using sodium hydroxide solution (0.3 M). Then, a solution of sodium borohydride (1.0 M, 10.5 mL) was added to the reaction mixture and stirred for 24 h at ambient temperature. The resulting black solid was separated from aqueous media using an external magnet, washed well with distilled H<sub>2</sub>O (3 × 20 mL) and EtOH (3 × 20 mL) and dried under vacuum at 50 °C for 4 h.

**General procedure for the Mizoroki–Heck cross-coupling reaction catalyzed by  $\gamma$ -Fe<sub>2</sub>O<sub>3</sub>-MBD/Pd-Co.**  $\gamma$ -Fe<sub>2</sub>O<sub>3</sub>-MBD/Pd-Co (0.05 mol% based on Pd) was added to a stirred suspension of haloarene (1 mmol), Et<sub>3</sub>N (2 mmol), alkene (1.3 mmol) in water (1 mL). The resulting mixture was heated at 60 °C. The reaction was monitored by TLC and, after the times shown in Table 3, the reaction was cooled down to room temperature. The organic compound was extracted twice with EtOAc (2 × 5 mL). The final organic layer was dried over MgSO<sub>4</sub> and filtered. Organic solvent evaporated under vacuum to give the crude product, which was purified by column chromatography (silica gel) using 50:1 volume ratio of *n*-hexane:EtOAc as eluent. The aqueous phase, containing the bimetallic catalyst, was again used for a new identical process.



**Scheme 1.** Synthesis of  $\gamma\text{-Fe}_2\text{O}_3\text{@MBD/Pd-Co}$ .

**General procedure for the Buchwald–Hartwig amination reaction of aryl iodides with arylamines catalyzed by  $\gamma\text{-Fe}_2\text{O}_3\text{-MBD/Pd-Co}$ .**  $\gamma\text{-Fe}_2\text{O}_3\text{-MBD/Pd-Co}$  (0.05 mol% based on Pd) was added to a stirred mixture of iodoarene (1 mmol), *t*-BuONa (2 mmol), and the arylamine (1.2 mmol) in  $\text{H}_2\text{O}$  (1 mL). The resulting suspension was heated at 50 °C and the reaction was monitored by TLC. After the times depicted in Table 6, the reaction mixture was cooled down. The organic product was extracted three times with EtOAc (3  $\times$  5 mL). The combined organic layers were dried over  $\text{MgSO}_4$  and the solvent evaporated under vacuum to give the crude product, which was purified by column chromatography (silica gel) using 10:1 volume ratio of *n*-hexane:EtOAc as eluent. The aqueous phase, containing the bimetallic catalyst, was again used for a new identical process.

**General procedure for the Buchwald–Hartwig amination reaction of aryl chlorides and bromides with arylamines catalyzed by  $\gamma\text{-Fe}_2\text{O}_3\text{-MBD/Pd-Co}$ .**  $\gamma\text{-Fe}_2\text{O}_3\text{-MBD/Pd-Co}$  (0.07 mol% based on Pd) was added to a stirred suspension of chloroarenes or bromoarenes (1 mmol), *t*-BuONa (2 mmol), and arylamines (1.2 mmol) in  $\text{H}_2\text{O}$  (1 mL). The resulting mixture was heated at 70 °C. The reaction was monitored by TLC and, after the times shown in Table 6, the reaction was cooled down to room temperature. The organic product was extracted three times with EtOAc (5 mL). The combined organic layers were dried over  $\text{MgSO}_4$  and the solvent was evaporated under vacuum to give the crude product, which was purified by column chromatography (silica gel) using 10:1 volume ratio of *n*-hexane:EtOAc as eluent. The aqueous phase, containing the bimetallic catalyst, was again used for a new identical process.

## Results and discussion

In Scheme 1, the approach which we have used for the preparation of Pd/Co bimetallic catalyst ( $\gamma\text{-Fe}_2\text{O}_3\text{@MBD/Pd-Co}$ ) is illustrated. In the first step,  $\gamma\text{-Fe}_2\text{O}_3$  was functionalized by the reaction with 3-chloro-trimethoxypropylsilane and subsequent treatment with melamine to produce  $\gamma\text{-Fe}_2\text{O}_3\text{-melamine}$  (Scheme 1, G0.5). The nucleophilic reaction of  $\gamma\text{-Fe}_2\text{O}_3\text{-melamine}$  with epichlorohydrin (ECH), as a bifunctional molecule for growing of dendritic branches afforded  $\gamma\text{-Fe}_2\text{O}_3\text{-melamine-ECH}$  (Scheme 1, G1). Ring opening reaction of terminal epoxides in  $\gamma\text{-Fe}_2\text{O}_3\text{-melamine-ECH}$  by melamine produced 1.5 generation of dendrimer-magnetite incorporation ( $\gamma\text{-Fe}_2\text{O}_3\text{@MBD}$ , G1.5). The last step involves the intercalating of metal complexes into the interior cavity of  $\gamma\text{-Fe}_2\text{O}_3\text{@MBD}$  followed by reduction with  $\text{NaBH}_4$  as a reducing agent.

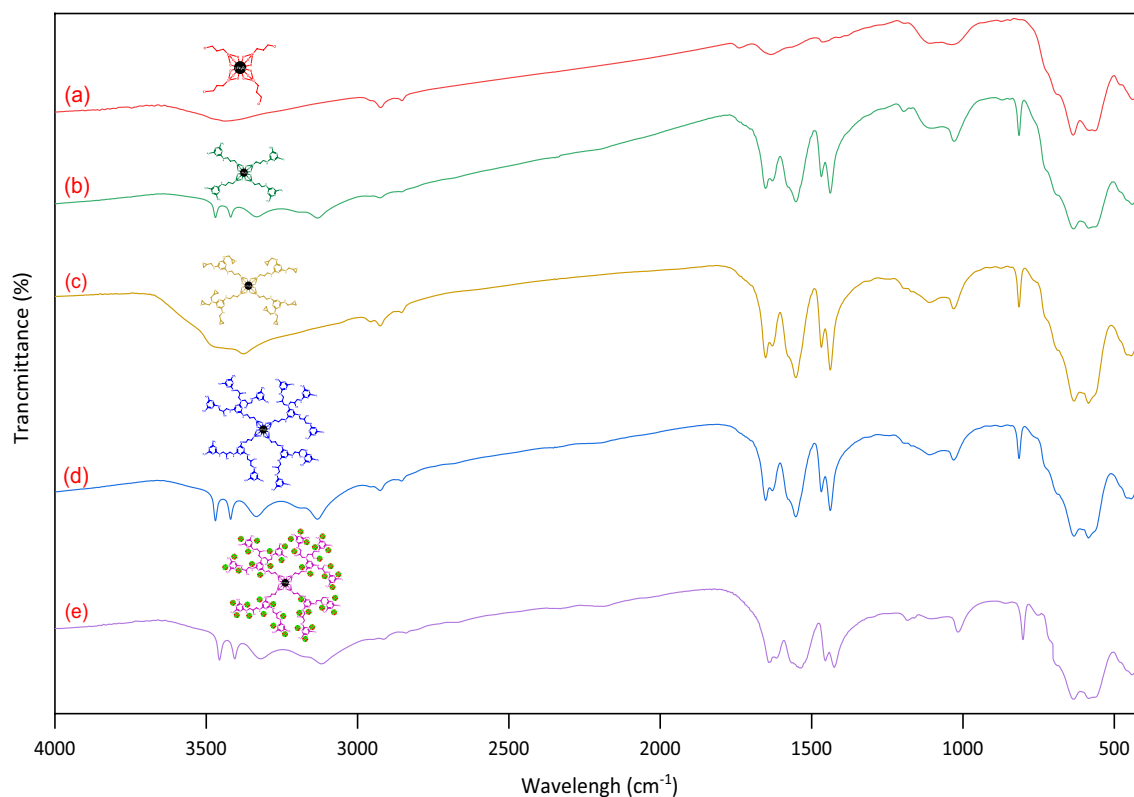


**Figure 1.** Plots of FT-IR spectra of (a) chlorofunctionalized  $\gamma$ - $\text{Fe}_2\text{O}_3$ , (b)  $\gamma$ - $\text{Fe}_2\text{O}_3$ -melamine, (c)  $\gamma$ - $\text{Fe}_2\text{O}_3$ -melamine-ECH, (d)  $\gamma$ - $\text{Fe}_2\text{O}_3$ @MBD and (e)  $\gamma$ - $\text{Fe}_2\text{O}_3$ @MBD/Pd-Co.

Chemical structures of all the new synthesized compounds (chlorofunctionalized  $\gamma$ - $\text{Fe}_2\text{O}_3$ ,  $\gamma$ - $\text{Fe}_2\text{O}_3$ -melamine,  $\gamma$ - $\text{Fe}_2\text{O}_3$ -melamine-ECH,  $\gamma$ - $\text{Fe}_2\text{O}_3$ @MBD and  $\gamma$ - $\text{Fe}_2\text{O}_3$ @MBD/Pd-Co) were determined via FT-IR spectroscopy (Fig. 1). FT-IR spectra of these compounds exhibited characteristic bands at around 563–636, 1037 and 3437  $\text{cm}^{-1}$  attributed to Fe–O, Si–O and O–H bonds, respectively. The FT-IR spectra of  $\gamma$ - $\text{Fe}_2\text{O}_3$ -melamine (Fig. 1b),  $\gamma$ - $\text{Fe}_2\text{O}_3$ @MBD (Fig. 1d) and  $\gamma$ - $\text{Fe}_2\text{O}_3$ @MBD/Pd-Co (Fig. 1e) exhibited typical bands at around 3471, 3415, 1651, 1550 and 814  $\text{cm}^{-1}$  attributed to N–H stretching and bending vibrations. In the FT-IR spectrum of  $\gamma$ - $\text{Fe}_2\text{O}_3$ -melamine-ECH (Fig. 1c), N–H band of primary amine vanished and new broad bands at 3471 and 3376  $\text{cm}^{-1}$  appeared. The new peaks were represented by the stretching vibration of N–H and O–H groups and proved that melamine and epichlorohydrine were effectively reacted. A slight shifting and variations in the amplitude of the N–H and C=N bands of triazine in Fig. 1e can justify the interaction of the metallic elements with the nitrogen atoms in the catalyst.

The metal content of  $\gamma$ - $\text{Fe}_2\text{O}_3$ @MBD/Pd-Co was calculated and quantified employing ICP analysis revealing 0.75 and 3.15 mmol of Pd and Co, respectively, (molar ratio Pd:Co = 1:4.2) per 1 g of the catalyst. Elemental analysis of  $\gamma$ - $\text{Fe}_2\text{O}_3$ -melamine and  $\gamma$ - $\text{Fe}_2\text{O}_3$ @MBD showed that the loadings of melamine on the catalyst were 9.88 and 17.50%, respectively, based on the nitrogen content.

As shown in Fig. 2, the XRD pattern of  $\gamma$ - $\text{Fe}_2\text{O}_3$ @MBD/Pd-Co established the crystalline structure of the bimetallic Pd-Co alloy nanoparticles. The sample exhibited characteristic diffraction peaks at  $2\theta = 30.3, 35.7, 43.4, 53.7, 57.2$  and  $62.9^\circ$ , which corresponded to the (2 2 0), (3 1 1), (4 0 0), (4 2 2), (5 1 1), and (4 4 0) reflections of the cubic maghemite<sup>29</sup>. The peaks at  $2\theta$  values of  $40.5, 46.4$  and  $67.90^\circ$  are due to the (1 1 1), (2 0 0), and (2 2 0) diffraction peaks corresponding to the face centered cubic Pd (JCPD-46-1043)<sup>10</sup>. The XRD pattern of the sample showed two diffraction signals were placed around  $2\theta = 44.8$  and  $47.5^\circ$  due to the Co species (JCPD-15-0806)<sup>30</sup>. However, those peaks mentioned above slightly shift to larger angles compared with the single metal counterpart<sup>30,31</sup>. The shift could be related to the bimetallic alloy formation.

Figure 3 depicts the thermogravimetric analysis of  $\gamma$ - $\text{Fe}_2\text{O}_3$ @MBD. In this plot the first weight loss of 1.18% (< 171  $^\circ\text{C}$ ), corresponded with the loss of physically adsorbed water. The second weight elimination of 11.61% (171–446  $^\circ\text{C}$ ) occurred as a consequence of degradation and decomposition of the organic material. These data justified that the melamine-based dendrimers are conveniently grafted on the magnetic nanoparticles. Magnetic properties of  $\gamma$ - $\text{Fe}_2\text{O}_3$ @MBD/Pd-Co and  $\gamma$ - $\text{Fe}_2\text{O}_3$  were surveyed employing a vibrating sample magnetometer (VSM) at room temperature (Fig. 4). Figure 4 revealed that the saturation magnetization value corresponding to  $\gamma$ - $\text{Fe}_2\text{O}_3$ @MBD/Pd-Co is approximately 59.07  $\text{emu g}^{-1}$ . The drop of the saturation magnetization of  $\gamma$ - $\text{Fe}_2\text{O}_3$ @MBD/Pd-Co compared with  $\gamma$ - $\text{Fe}_2\text{O}_3$  (76.48  $\text{emu g}^{-1}$ ) was related to the coating of  $\gamma$ - $\text{Fe}_2\text{O}_3$  by melamine-based dendrimer. The magnetization curves did not show a hysteresis loop, which justified the superparamagnetic nature of the resulting NPs. High magnetic properties of NPs were appropriate for their further recovery from the reaction media by the simple magnetic separation using a conventional magnet.

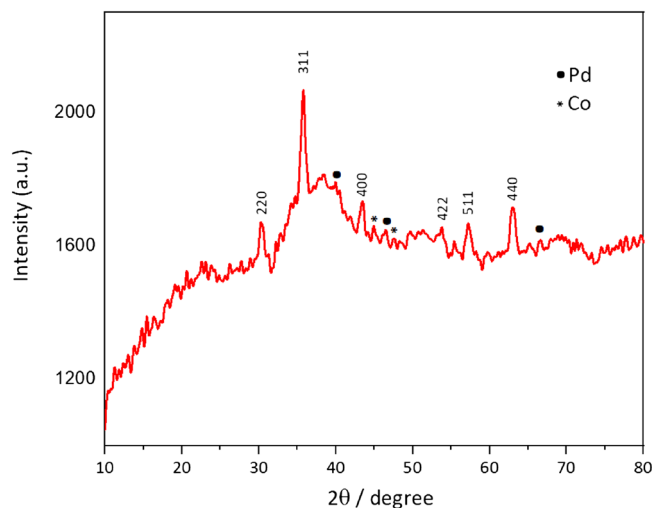


**Figure 2.** The XRD pattern of  $\gamma\text{-Fe}_2\text{O}_3\text{@MBD/Pd-Co}$ .

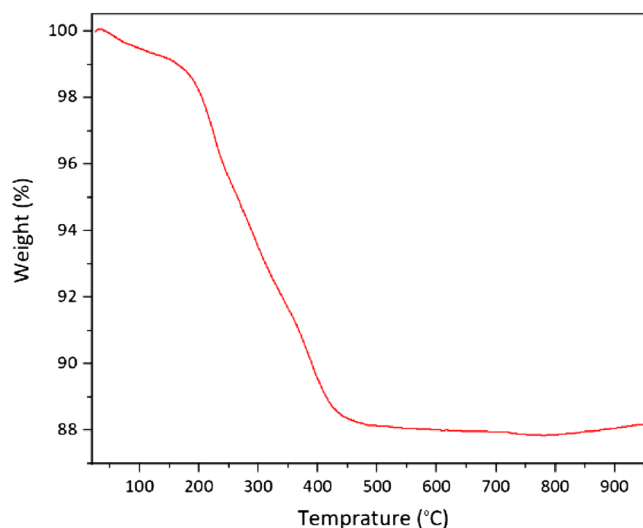


**Figure 3.** The TG analysis of  $\gamma\text{-Fe}_2\text{O}_3\text{@MBD/Pd-Co}$ .

A deep XPS analysis was done to characterize the chemical composition of  $\gamma\text{-Fe}_2\text{O}_3\text{@MBD/Pd-Co}$  surface (Fig. 5). The peaks associated to carbon, nitrogen, oxygen, silicon, iron, palladium and cobalt are evidently detected in the XPS plot (Fig. 5a). The C1s spectrum (Fig. 5b) showed binding energies at 284.5 (C<sub>sp2</sub>-N and C-C), 286.0 (C-O and C=N), and 288.1 (C-N) eV<sup>32,33</sup>. Deconvolution of N<sub>1s</sub> region showed two peaks at 398.0 and 399.5 eV corresponding to C=N=C and N-H, respectively (Fig. 5c)<sup>34</sup>. In Fig. 5d, the peaks at 335.1 (3d<sub>5/2</sub>) and 340.4 eV (3d<sub>3/2</sub>), corresponded to Pd in the zero oxidation state. The peaks at 336.6 (3d<sub>5/2</sub>) and 341.8 eV (3d<sub>3/2</sub>) indicated that a small amount of Pd presents in (II) oxidation state<sup>35,36</sup>. The typical peaks located at 780.6 (2p<sub>3/2</sub>) and 796.4 eV (2p<sub>1/2</sub>) revealed the presence of cobalt (0) in the catalyst (Fig. 5e). It was also detected the presence of both weaker peaks at 782.6 (2p<sub>3/2</sub>) and 798.4 eV (2p<sub>1/2</sub>) corresponding to cobalt (II) species. Different weak satellite peaks at 785.8, 788.6, 801.3 and 803.0 eV<sup>30</sup>, showed the existence of Co<sub>3</sub>O<sub>4</sub> on the catalyst surface<sup>37</sup>. The displacement of the 2p<sub>3/2</sub> signal of cobalt to a lower energy and a positive shift in the 3d<sub>5/2</sub> peak of Pd indicated the alloying of Co with Pd<sup>38</sup>. Moreover, the atomic distribution of palladium *versus* cobalt in the surface of  $\gamma\text{-Fe}_2\text{O}_3\text{@MBD/Pd-Co}$  is 1:8.45, which is notably higher than the stoichiometric value (1:4.2) calculated by ICP analysis. This larger value demonstrates that the bimetallic Pd-Co nanoparticles generates a core-shell structure with a cobalt-rich shell and a palladium-rich core<sup>39,40</sup>, and consequently, a larger cobalt surface is exposed.

The morphology of the surface and size of the particles of the freshly prepared new catalyst were analyzed by transmission electron microscopy (TEM) (Fig. 6). In Fig. 6a a spherical morphology of  $\gamma\text{-Fe}_2\text{O}_3$  magnetic nanoparticles was shown. Comparing TEM image of  $\gamma\text{-Fe}_2\text{O}_3\text{@MBD/Pd-Co}$  (Fig. 6b) with  $\gamma\text{-Fe}_2\text{O}_3$  showed that dendrimer-magnetite incorporation was dispersed considerably. Figure 6e shows an average diameter size of ~12 nm for  $\gamma\text{-Fe}_2\text{O}_3\text{@MBD/Pd-Co}$ . Characteristic lattice fringes for 2 2 0 planes of  $\gamma\text{-Fe}_2\text{O}_3$  with a d-spacing of

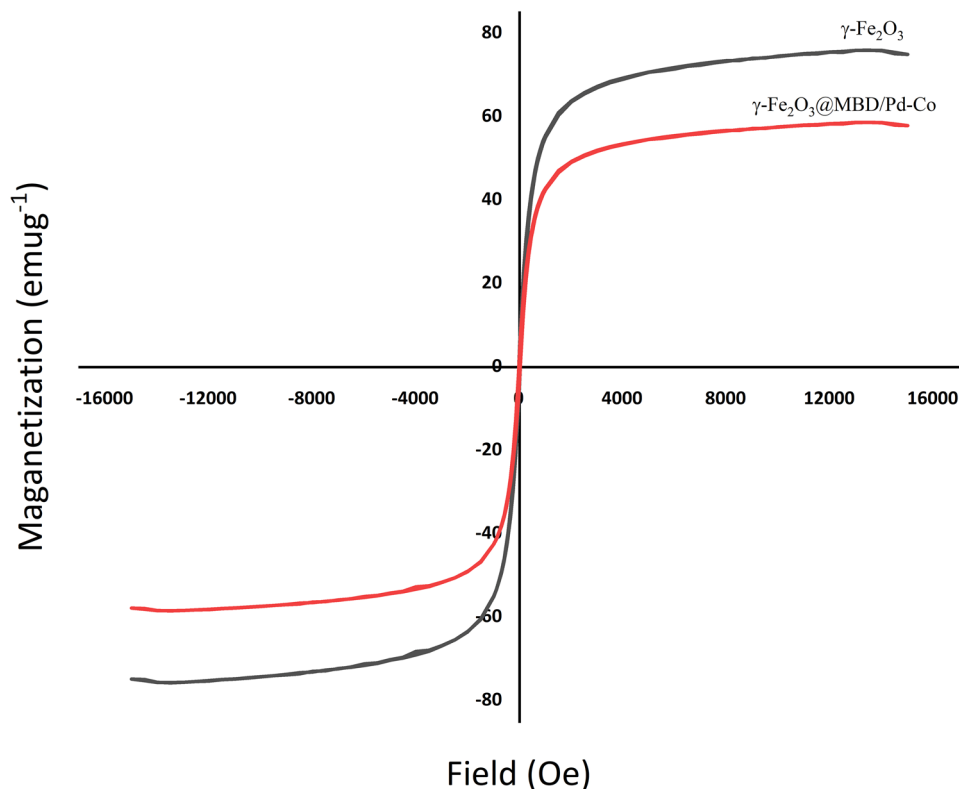


**Figure 4.** The VSM pattern of  $\gamma\text{-Fe}_2\text{O}_3\text{@MBD/Pd-Co}$  and  $\gamma\text{-Fe}_2\text{O}_3$ .

0.28 nm recognized in Fig. 6c. Moreover, TEM images, revealed a homogeneous spreading of the cobalt and palladium alloy nanoparticles immobilized onto the  $\gamma\text{-Fe}_2\text{O}_3\text{@MBD}$  surface (Fig. 6c). The size distribution histogram of palladium and cobalt alloy nanoparticles (Fig. 6f), illustrated a high size uniformity of the detected spherical nanoparticles with diameter of about  $\sim 3\text{--}5$  nm. Figure 6d depicted the lattice fringe spacing  $\sim 3.26\text{--}3.71$  Å related to the Pd-Co alloy nanoparticles<sup>41–43</sup>.

The EDS elemental mapping images of the  $\gamma\text{-Fe}_2\text{O}_3\text{@MBD/Pd-Co}$  are presented in Fig. 7. The EDS images prove the presence of the Fe, Co and Pd elements on the  $\gamma\text{-Fe}_2\text{O}_3\text{@MBD/Pd-Co}$  surface. As it is observed in the Fig. 7, cobalt is denser than palladium on the surface of it.

**Mizoroki–Heck cross-coupling reaction catalyzed by  $\gamma\text{-Fe}_2\text{O}_3\text{@MBD/Pd-Co}$  in water.** Mizoroki–Heck cross-coupling reactions are applied for the preparation of natural products, pharmaceuticals and biologically active molecules<sup>3,44–46</sup>. These reactions, involving the generation of new carbon–carbon bonds formation, have found several commercial applications for the synthesis of fine chemicals such as herbicide prosulfuron, anti-inflammatory naproxen, or anti-asthma agent Singulair in the multi-ton scale in each year<sup>47</sup>. Generally, the Mizoroki–Heck cross-coupling reaction is catalyzed by palladium complexes<sup>48</sup>. However, another transition metals such as Ni<sup>49</sup>, Co<sup>50</sup> and Cu<sup>51</sup> have been recently reported as catalysts for this purpose. Due to the advantageous of bimetallic catalysts such as enhanced catalytic activity which comes from the synergistic effect of the monometallic counterparts, in the past decades, some bimetallic catalysts such as Pd/Cu<sup>52</sup>, Pd/Pt<sup>53</sup>, Pd/Co<sup>11</sup>, Pd/Au<sup>54</sup>, Pd/Ni<sup>55</sup>, Pd/Fe<sup>56</sup> and etc. have been developed for the Mizoroki–Heck cross-coupling reaction. The synthetic routes published in the literature have certain limitations due to the necessary high temperature, the large amount of catalyst loading, the introduction of additives, the employment of organic solvents and the use of an unrecyclable catalyst. In addition, most of the reported methods suffered from lack of generality for the coupling reactions employing chloroarenes. Continuing with our research on the design and the preparation of novel and attractive catalytic systems to conduct environmentally friendly cross-coupling reactions<sup>4</sup>, herein, we have surveyed the catalytic activity of a novel  $\gamma\text{-Fe}_2\text{O}_3\text{@MBD/Pd-Co}$  as the first magnetically recyclable Pd/Co bimetallic catalyst in the Mizoroki–Heck coupling reactions.

At first, the coupling reaction of iodobenzene with *n*-butyl acrylate (1:1.3 molar ratio) in water was investigated as a bench reaction to optimize the effect of the catalyst loading, type of the base and temperature on the reaction completion (Table 1). In the preliminary studies, this model reaction was investigated in the presence of variable amounts of  $\gamma\text{-Fe}_2\text{O}_3\text{@MBD/Pd-Co}$  using  $\text{Et}_3\text{N}$  as the base (2 equiv.) at 60 °C (Table 1, entries 1–3). The best amount of the catalyst was 0.05 mol% (Table 1, entry 3). The reaction did not work when any amount of the catalyst was not used (Table 1, entry 4). This result proved the crucial role of the catalyst for this transformation. Several bases such as  $\text{K}_2\text{CO}_3$ ,  $\text{CsCO}_3$ ,  $\text{Na}_2\text{CO}_3$ ,  $\text{NaHCO}_3$ , KOH and NaOEt were examined for the model reaction using 0.05 mol% of the catalyst at 60 °C (Table 1, entries 5–10). Within the bases tested,  $\text{Et}_3\text{N}$  was found to be the

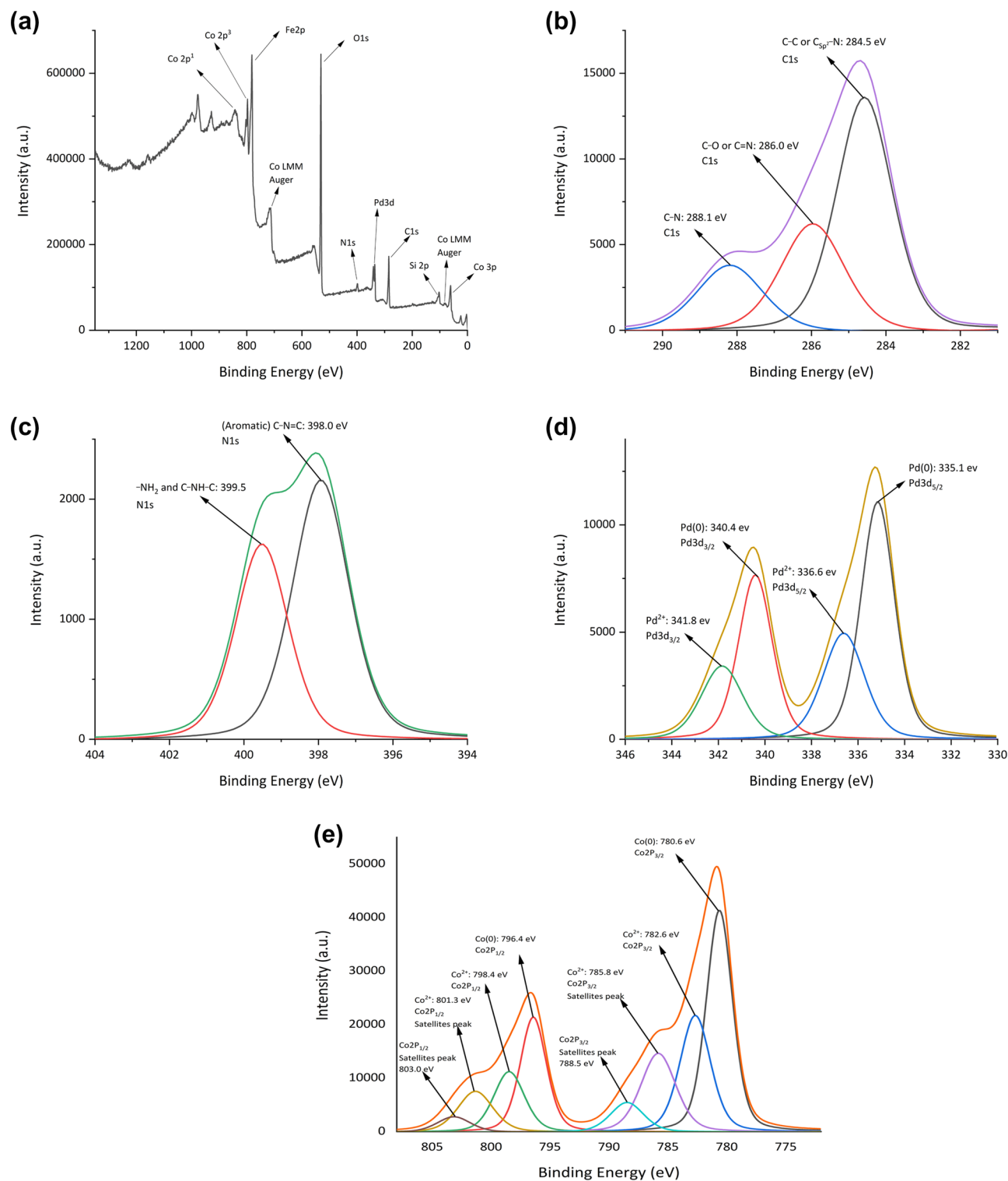


**Figure 5.** (a) XPS analysis of  $\gamma$ -Fe<sub>2</sub>O<sub>3</sub>@MBD/Pd-Co, (b) C 1s, (c) N 1s, (d) Pd 3d and (e) Co 2p.

most effective base (Table 1, entry 3). When no bases was used, the corresponding product was obtained with a desirable yield (Table 1, entry 11), which showed that the intrinsic basic sites of melamine-based dendrimer may also promote the reaction in some extent. Subsequently, the reaction was attempted at lower temperatures (Table 1, entries 12 and 13). Here, the product was produced in very low yields and using longer reaction times, especially when the reaction was carried out at room temperature.

The coupling reaction of iodobenzene with *n*-butyl acrylate (1:1.3 molar ratio) under optimized reaction conditions was also studied in the presence of the catalyst containing different ratios of Pd:Co (Table 2). As the ratio of Pd:Co is changed from 1:5.8 to 1:4.2, the efficiency of the catalyst is increased (entry 2). This could be

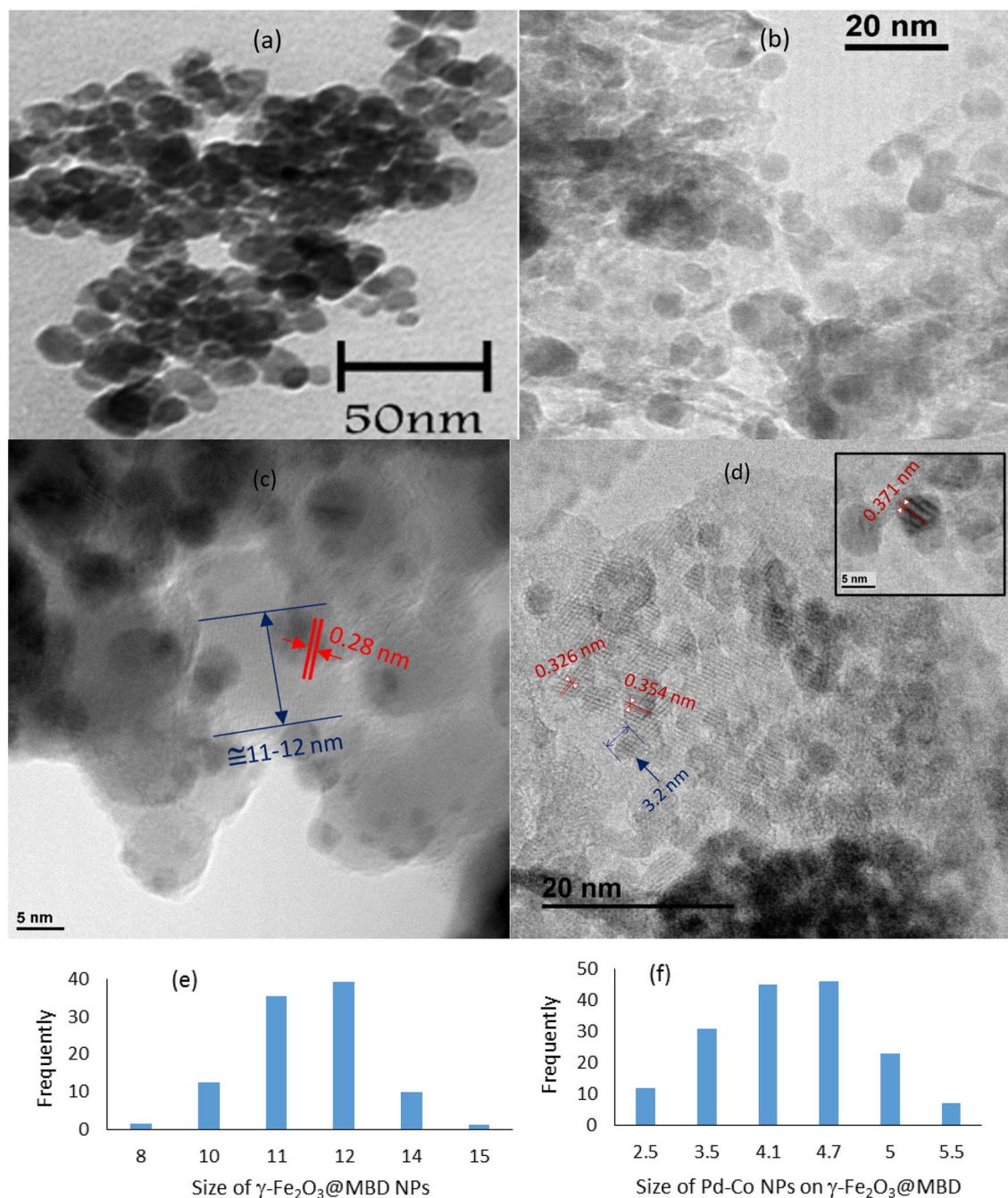


**Figure 6.** The TEM images of (a)  $\gamma\text{-Fe}_2\text{O}_3$  and (b–d)  $\gamma\text{-Fe}_2\text{O}_3\text{@MBD/Pd-Co}$  and (e) the particle size distribution of  $\gamma\text{-Fe}_2\text{O}_3\text{@MBD/Pd-Co}$  and (f) the particle size distribution of Pd-Co nanoparticles on the  $\gamma\text{-Fe}_2\text{O}_3\text{@MBD}$  surface.

related to increasing the amount of Pd as the most active species in the catalyst. Performing similar reaction in the presence of  $\gamma\text{-Fe}_2\text{O}_3\text{@MBD/Pd-Co}$  containing Pd:Co (1:0.8, entry 3) produced the desired product with the same yield as  $\gamma\text{-Fe}_2\text{O}_3\text{@MBD/Pd-Co}$  containing Pd:Co (1:4.2). Therefore, the optimum molar ratio of Pd:Co in the catalyst should be 1:4.2.

Using the optimized reaction conditions, the scope of Mizoroki–Heck cross-coupling reaction catalyzed by  $\gamma\text{-Fe}_2\text{O}_3\text{@MBD/Pd-Co}$  was investigated by employing various aryl halides to react with olefins in water (Table 3). The results of Table 3 reveal that this catalytic protocol is very efficient for running coupling reaction of tested haloarenes. It is worth to mention that any homo-coupling reaction was not occurred in all of the reactions tested. Iodoarenes were coupled with assorted alkenes such as alkyl acrylates and methyl methacrylate following the optimal reaction conditions obtaining the desired products in 95–99% yields (Table 3, entries 1–6). Bromo- and chloroarenes, underwent satisfactory coupling reactions with *n*-butyl acrylate furnishing products in good to



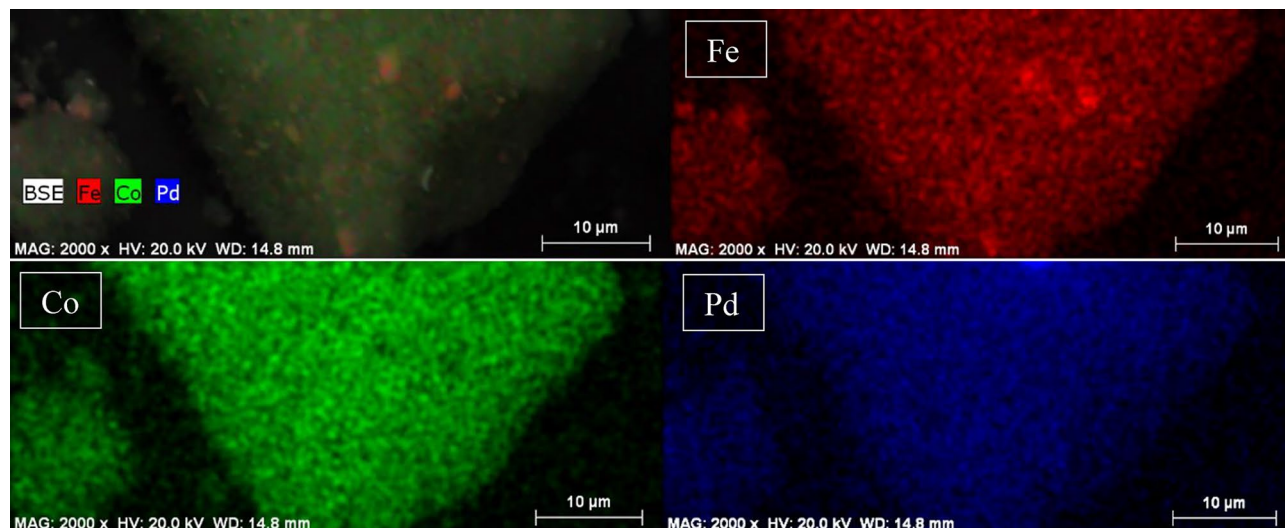


**Figure 7.** EDS elemental mapping images of the  $\gamma$ -Fe<sub>2</sub>O<sub>3</sub>@MBD/Pd-Co.

Entry <sup>[a]</sup>	Catalyst (mol%) <sup>[b]</sup>	Base	Time (min)	Isolated yield (%)
1	0.03	Et <sub>3</sub> N	60	91
2	0.04	Et <sub>3</sub> N	60	97
3	0.05	Et <sub>3</sub> N	25	99
4	–	Et <sub>3</sub> N	24 h	Trace
5	0.05	K <sub>2</sub> CO <sub>3</sub>	75	92
6	0.05	CsCO <sub>3</sub>	65	85
7	0.05	Na <sub>2</sub> CO <sub>3</sub>	120	85
8	0.05	NaHCO <sub>3</sub>	120	81
9	0.05	KOH	85	78
10	0.05	NaOEt	30	92
11	0.05	–	70	91
12 <sup>[c]</sup>	0.05	Et <sub>3</sub> N	60	93
13 <sup>[d]</sup>	0.05	Et <sub>3</sub> N	24 h	65

**Table 1.** Mizoroki–Heck reaction between iodobenzene and *n*-butyl acrylate catalyzed by  $\gamma$ -Fe<sub>2</sub>O<sub>3</sub>@MBD/Pd-Co using water. [a] Reaction conditions: iodobenzene (1 mmol), *n*-butyl acrylate (1.3 mmol), base (2 mmol), water (1 mL), 60 °C (except for entries 12 and 13), [b] based on the Pd content, [c] 50 °C, [d] room temperature.

Entry <sup>[a]</sup>	Pd <sup>[a]</sup> (mmol g <sup>-1</sup> )	Co <sup>[a]</sup> (mmol g <sup>-1</sup> )	molar ratio Pd:Co	Pd (mol%)	Time (min)	Isolated yield <sup>[b]</sup> (%)
1	0.593	3.44	1:5.8	0.04	540	95
2	0.751	3.15	1:4.2	0.05	25	99
3	1.61	1.29	1:0.8	0.1	20	99

**Table 2.** Mizoroki–Heck reaction between iodobenzene and *n*-butyl acrylate catalyzed by  $\gamma$ -Fe<sub>2</sub>O<sub>3</sub>@MBD/Pd-Co containing different ratios of Pd:Co in water. [a] Based on ICP-OES analysis, [b] Reaction conditions: iodobenzene (1 mmol), *n*-butyl acrylate (1.3 mmol), base (2 mmol), water (1 mL), 60 °C, catalyst (0.00066 g).

Entry	Aryl halide	Olefins	Product	Time (min)	Isolated yield <sup>[a]</sup> (%)
1				25	99
2				35	95
3				20	98
4				30	99
5				55	95
6				30	98
7				120	98
8				120	97
9				90	95
10				240	99
11				210	90
12				240	95
13				70	98
14				65	95
15				120	95
16				215	90
17				55	95
18				130	90
19				120	90

**Table 3.** Mizoroki–Heck reaction of various haloarenes with olefins promoted by  $\gamma$ - $\text{Fe}_2\text{O}_3$ @MBD/Pd-Co in aqueous media. [a] Reaction conditions: catalyst (0.05 mol% based on the Pd content), haloarene (1 mmol), alkene (1.3 mmol),  $\text{Et}_3\text{N}$  (2 mmol), water (1 mL), 60 °C. Trans-isomer was identified based on  $^3J_{\text{H-H}}$  value of 16.0–16.4 Hz for vinylic hydrogens in the  $^1\text{H}$  NMR of the products (Figure S1–S13).

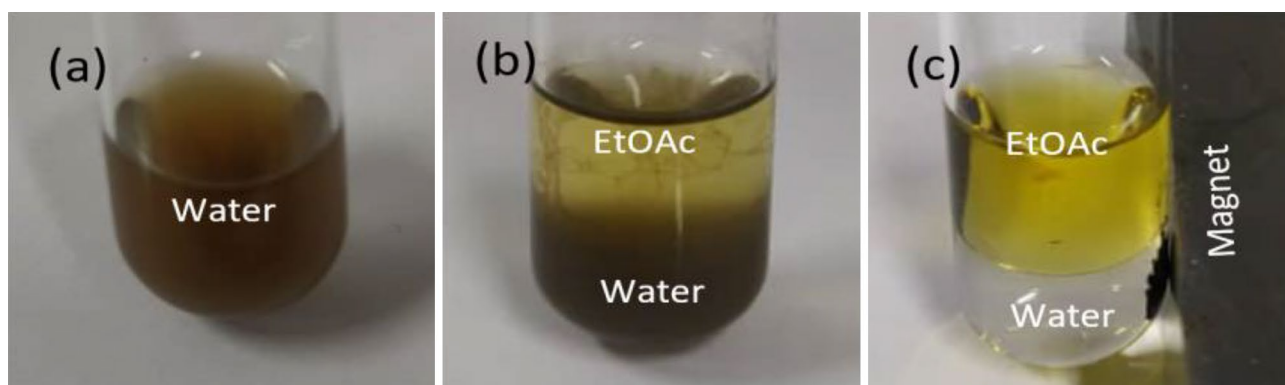


**Figure 8.** (a) Dispersion of  $\gamma\text{-Fe}_2\text{O}_3\text{@MBD/Pd-Co}$  in the aqueous media, (b) distribution of  $\gamma\text{-Fe}_2\text{O}_3\text{@MBD/Pd-Co}$  in water/EtOAc and (c) isolation of  $\gamma\text{-Fe}_2\text{O}_3\text{@MBD/Pd-Co}$  by an external magnet.

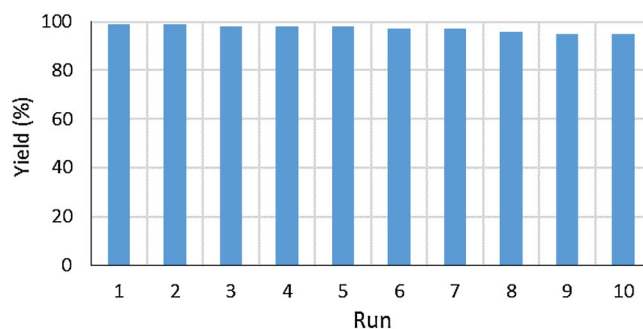


**Figure 9.** Reusability of  $\gamma\text{-Fe}_2\text{O}_3\text{@MBD/Pd-Co}$  in the reaction of *n*-butyl acrylate (1.3 mmol) with chlorobenzene (1 mmol) in the presence of  $\gamma\text{-Fe}_2\text{O}_3\text{@MBD/Pd-Co}$  (0.05 mol% based on the Pd content), base (2 mmol) in water (1 mL) in 4 h.

high yields (Table 3, entries 7–12). Moreover, a variety of aryl halides underwent successful coupling reaction with styrene under optimized reaction conditions (Table 3, entries 13–19).

Since the recovery and recycling of the supported catalysts are very important issues from both the practical and environmental point of view, the reusability of the catalyst in the model reaction was investigated under optimized reaction conditions. Due to the nitrogen and hydroxyl groups in  $\gamma\text{-Fe}_2\text{O}_3\text{@MBD/Pd-Co}$ , the catalyst was dissolved in the aqueous layer with no affinity to the organic layer (Fig. 8). According to this feature, the product was extracted with ethyl acetate, while the catalyst remained in the aqueous layer (Fig. 8b). The aqueous layer containing the catalyst was allowed to react with a new batch of iodobenzene, *n*-butyl acrylate and  $\text{Et}_3\text{N}$ . At the end, the catalyst was separated from the aqueous phase employing a magnet (Fig. 8c). The catalytic activity of the recovered catalyst was identical to the original one, and the same behavior took place after ten runs (Fig. 9). FT-IR spectrum, XPS pattern and TEM images of the catalyst recovered after the tenth reaction, indicated that the catalyst remained unchanged (Fig. 10).

The heterogeneous nature of the catalyst was checked by the hot filtration and poisoning tests. In the hot filtration test, after approximate 40% of the coupling reaction of chlorobenzene with *n*-butylacrylate, the solid was separated at the reaction temperature using an external magnetic field and the reaction was permitted to stir for 4 h. Any additional transformation indicated that the catalysis was heterogeneous in nature (Fig. 11). In the poisoning test,  $\text{S}_8$  (0.07 g) was used as a scavenger for the metal. Under this condition, any considerable change in the progress of the reaction was not observed.

**C-N cross-coupling reaction catalyzed by  $\gamma\text{-Fe}_2\text{O}_3\text{@MBD/Pd-Co}$  in water.** Arylamines and their derivatives possess a paramount importance as intermediates for pharmaceuticals and natural products, agrochemicals, conducting polymers (PANI), and dyes in the chemical industry<sup>57–59</sup>. Arylamines are extremely important ligand for the coordination to transition metals<sup>60</sup>. The Buchwald–Hartwig coupling of amines and aryl halides in the presence of Pd is a great method for the preparation of arylamines<sup>61–63</sup>. Since the discovery of Buchwald–Hartwig amination reaction<sup>64</sup>, research efforts have concentrated on this reaction and significant development have been achieved on the improvement of the conventional reaction conditions such as using diverse transition metals, ligands, and solvents as well as extending substrate scope<sup>65</sup>. The importance of bimetallic catalysts in organic synthesis has recently encouraged organic chemists to use these kinds of catalysts in coupling reactions. Along this line, Fe@Pd nanowire<sup>66</sup>, Pd/Ni nanoparticles<sup>67</sup> and Pd/Cu complexes<sup>68</sup> have been used as bimetallic catalysts for the C–N coupling reactions. Encouraged by the facile Mizoroki–Heck cross-coupling reaction catalyzed by  $\gamma\text{-Fe}_2\text{O}_3\text{@MBD/Pd-Co}$ , we have tried our catalyst for C–N coupling reaction as well.

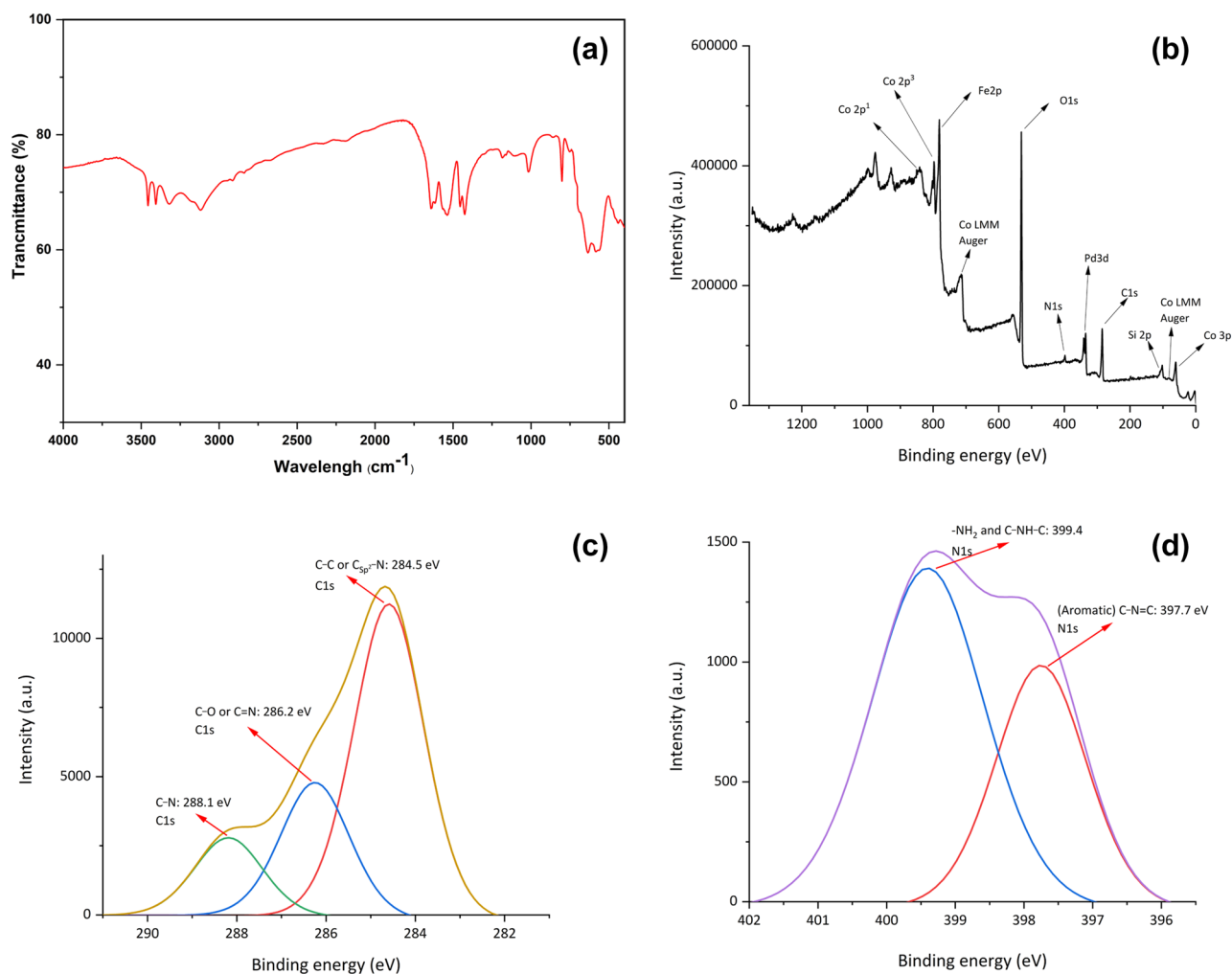


**Figure 10.** (a) FT-IR spectrum, (b) XPS pattern, (c) C 1s, (d) N 1s, (e) Pd 3d, (f) Co 2p and (g,h) TEM images of recycled  $\gamma\text{-Fe}_2\text{O}_3\text{@MBD/Pd-Co}$  after ten reaction runs.

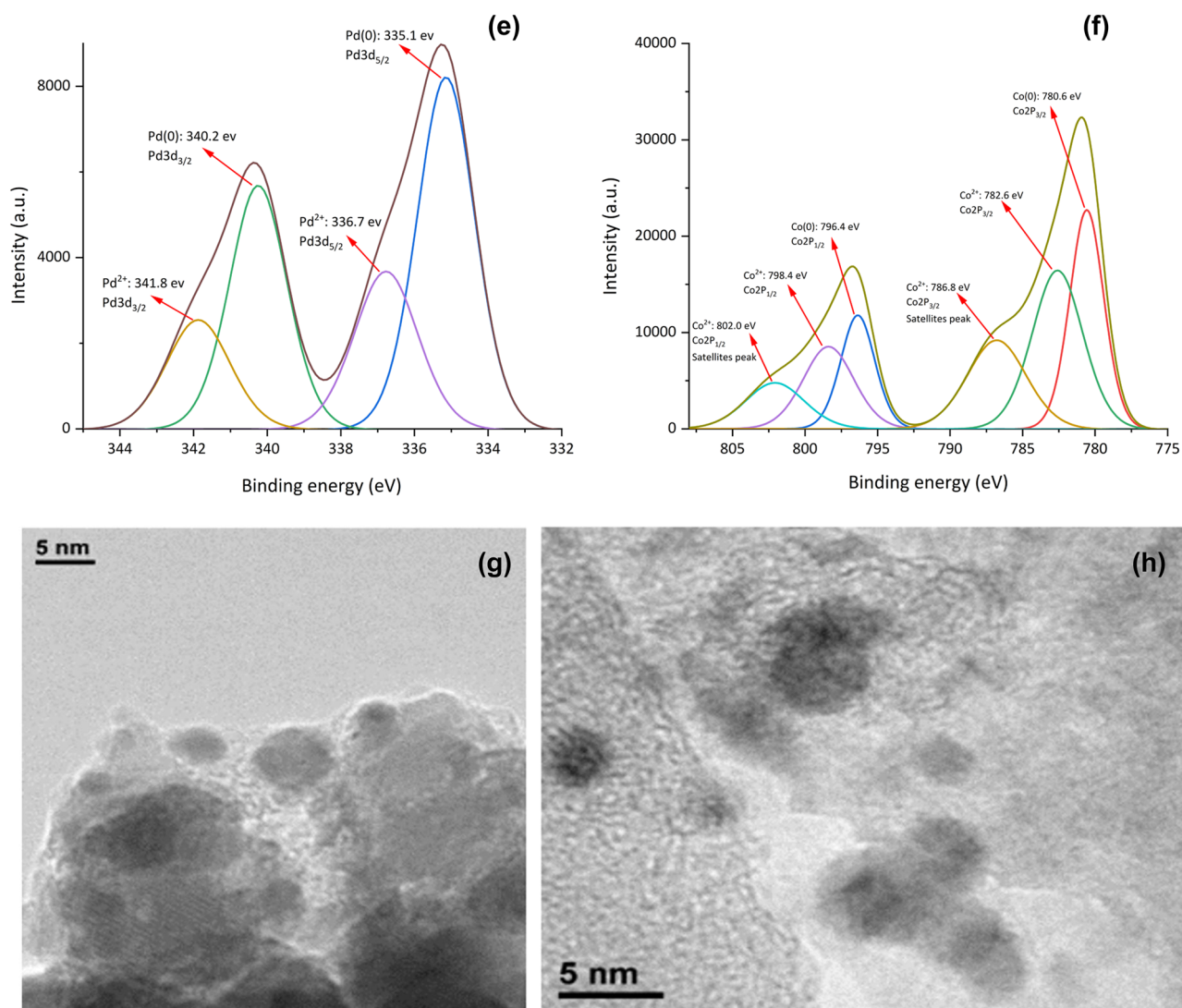


**Figure 10.** (continued)

Surprisingly, to the best of our knowledge, there is not any report on the Buchwald–Hartwig amination reaction catalyzed by Pd/Co bimetallic nanoparticles.

To investigate the catalytic activity of the  $\gamma$ -Fe<sub>2</sub>O<sub>3</sub>@MBD/Pd-Co toward the Buchwald–Hartwig amination reaction, the cross-coupling reaction of chlorobenzene as a poor reactive aryl donor, with aniline in aqueous media, was selected as a bench reaction. Several reaction factors such as the catalyst loading, base and temperature were screened. The results are collected in Table 4. As it is remarked in Table 4, the best yield of the product was observed when 0.07 mol% of the catalyst was used (Table 4, entry 2). Among all the tested organic and inorganic bases (Table 4, entries 6–9), *t*-BuONa was found to be the most effective base. When any bases was not used, the product was isolated in 54% yield after 24 h (Table 4, entry 10), which showed that the intrinsic basic sites of melamine-based dendrimer may also promote the reaction. The model reaction was studied at different temperatures (Table 4, entries 11–13) and the greatest yield of the desired product was produced at 80 °C (Table 4, entry 2). The assessment of the temperature and the catalyst loading was also done for iodobenzene as a highly reactive aryl donor in Table 5. The information given by all these experiments confirmed that 0.05 mol% of the catalyst and 50 °C are the most appropriate conditions to complete the reaction successfully (Table 5, entry 3).

Next, the chemical scope of this novel bimetallic catalyst was explored and the results are summarized in Table 6. Many aryl iodides were coupled with different arylamines in the presence of  $\gamma$ -Fe<sub>2</sub>O<sub>3</sub>@MBD/Pd-Co and *t*-BuONa under optimized reaction conditions (0.05 mol% of the catalyst, 50 °C) and the corresponding products were obtained in 82–93% yields (Table 6, entries 1–6). The coupling reaction of bromo- and chloroarenes with several arylamines was fruitful using 0.07 mol% of the catalyst at 80 °C (Table 6, entries 7–15).

The Mizoroki–Heck and Buchwald–Hartwig amination reactions of chlorobenzene with *n*-butyl acrylate and aniline, respectively, catalyzed by monometallic counterparts including  $\gamma$ -Fe<sub>2</sub>O<sub>3</sub>@MBD/Pd,  $\gamma$ -Fe<sub>2</sub>O<sub>3</sub>@MBD/Co, Fe<sub>2</sub>O<sub>3</sub>@MBD/Pd(OAc)<sub>2</sub>,  $\gamma$ -Fe<sub>2</sub>O<sub>3</sub>@MBD/CoCl<sub>2</sub>, physical mixture of  $\gamma$ -Fe<sub>2</sub>O<sub>3</sub>@MBD/Pd and  $\gamma$ -Fe<sub>2</sub>O<sub>3</sub>@MBD/Co, Pd(OAc)<sub>2</sub>, CoCl<sub>2</sub>·6H<sub>2</sub>O, and Fe<sub>2</sub>O<sub>3</sub>@MBD/Co<sub>3</sub>O<sub>4</sub> were also investigated and the results were compared with the bimetallic catalyst ( $\gamma$ -Fe<sub>2</sub>O<sub>3</sub>@MBD/Pd-Co) (Fig. 12). Obviously, the bimetallic particles provided higher

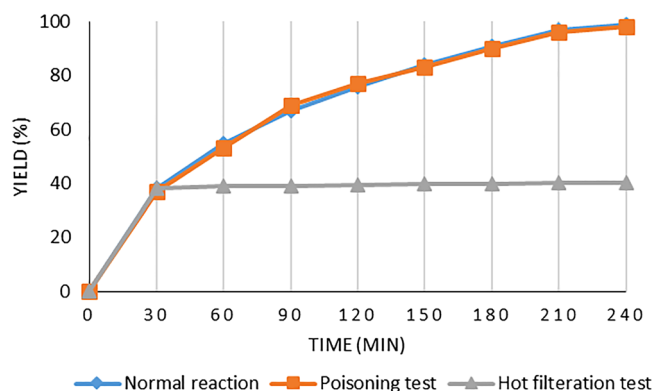


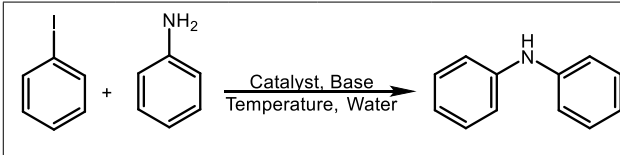
**Figure 11.** Studies of the heterogeneity of  $\gamma\text{-Fe}_2\text{O}_3\text{@MBD/Co-Pd}$ .

Entry <sup>[a]</sup>	Catalyst (mol%) <sup>[b]</sup>	Base	Time(h)	Isolated yield (%)
1	0.1	<i>t</i> -BuONa	4	87
2	0.07	<i>t</i> -BuONa	5	90
3	–	<i>t</i> -BuONa	24	0
4	0.05	<i>t</i> -BuONa	10	80
5	0.04	<i>t</i> -BuONa	12	75
6	0.07	EtONa	6	83
7	0.07	K <sub>2</sub> CO <sub>3</sub>	24	23
8	0.07	KOH	24	39
9	0.07	Et <sub>3</sub> N	24	56
10	0.07	–	24	54
11 <sup>[c]</sup>	0.07	<i>t</i> -BuONa	4	90
12 <sup>[d]</sup>	0.07	<i>t</i> -BuONa	8	81
13 <sup>[e]</sup>	0.07	<i>t</i> -BuONa	24	Trace

**Table 4.** Buchwald–Hartwig amination reaction of chlorobenzene with aniline catalyzed by  $\gamma\text{-Fe}_2\text{O}_3\text{@MBD/Pd-Co}$  under different conditions in water. [a] Reaction conditions: chlorobenzene (1 mmol), aniline (1.2 mmol), water (1 mL), 80 °C (except for entries 11–13), [b] based on the Pd content, [c] 100 °C, [d] 70 °C, [e] room temperature.

chemical yield (99%) compared with the monometallic counterparts in both reduced and nonreduced forms, physical mixture of monometallic counterparts, and non-supported metal salts and also supported cobalt oxide. The enhanced catalytic activity of these new species is probably originated by a synergistic effect of both metals.

Based on the results and fully characterization of the catalyst and other previous contributions<sup>11,69</sup>, we tentatively proposed a plausible mechanisms for Mizoroki–Heck and Buchwald–Hartwig amination reactions in the presence of  $\gamma\text{-Fe}_2\text{O}_3\text{@MBD/Pd-Co}$  (Scheme 2). As it is clear in Fig. 12, the Mizoroki–Heck and Buchwald–Hartwig amination reactions proceeded with higher efficiency when involved  $\gamma\text{-Fe}_2\text{O}_3\text{@MBD/Pd-Co}$  as a bimetallic catalyst than monometallic counterparts. These finding are in good agreements with a negative shift of the 2p<sub>3/2</sub> peak of Co and a positive shift in the 3d<sub>5/2</sub> peak of Pd in the XPS analysis (Fig. 5). The peak shifts indicate that the neighbouring cobalt atoms contribute to increase the electronic density of Pd centres and facilitates the oxidative addition of haloarenes to Pd (0)<sup>11</sup>. Evidently, this step in the coupling reactions is responsible for the higher activity of bimetallic catalysts compared with monometallic counterparts. In the proposed mechanism shown in Scheme 2, at first, the Pd-Co alloy underwent oxidative addition with haloarenes to form an organometallic intermediate I on the surface of the catalyst. Then, the reaction proceeds by coordination of olefin or aniline to the intermediate I to form intermediate II and III, respectively. *Syn*-migratory insertion in intermediate II generated intermediate complex IV, which undergoes *syn*-β-hydride elimination to afford the



Entry <sup>[a]</sup>	Base	T (°C)	Time (h)	Isolated yield (%)
1 <sup>[b]</sup>	<i>t</i> -BuONa	80	3	88 <sup>[c]</sup>
2	<i>t</i> -BuONa	80	3	89 <sup>[c]</sup>
3	<i>t</i> -BuONa	50	4	92
4	<i>t</i> -BuONa	40	6	85
5	<i>t</i> -BuONa	r.t.	24	70
6 <sup>[d]</sup>	<i>t</i> -BuONa	50	24	0
7	EtONa	50	5	86
8	K <sub>2</sub> CO <sub>3</sub>	50	24	47
9	KOH	50	24	41
10	Et <sub>3</sub> N	50	24	71

**Table 5.** Buchwald–Hartwig amination reaction of iodobenzene with aniline catalyzed by  $\gamma$ -Fe<sub>2</sub>O<sub>3</sub>@MBD/Pd-Co under different conditions in water. [a] Reaction conditions: iodobenzene (1 mmol), aniline (1.2 mmol), water (1 mL), 0.05 mol% of  $\gamma$ -Fe<sub>2</sub>O<sub>3</sub>@MBD/Pd-Co based on the Pd content (except entry 1 and 6), [b] 0.07 mol% of  $\gamma$ -Fe<sub>2</sub>O<sub>3</sub>@MBD/Pd-Co based on the Pd content, [c] Biaryl as a by-product was also obtained, [d] Without any catalyst.

Mizoroki–Heck coupling product. Finally, the base-assisted elimination of H–X from species **V** occurred to regenerate the catalyst. In the suggested mechanism for Buchwald–Hartwig amination reactions, the product is formed through the base-assisted elimination of H–X from intermediate **III** by subsequent reductive elimination.

Finally, the catalytic activity of  $\gamma$ -Fe<sub>2</sub>O<sub>3</sub>@MBD/Pd-Co was compared with those of reported Pd bimetallic catalysts in the Mizoroki–Heck and Buchwald–Hartwig amination reactions (Table 7). As summarized in Table 7, the most efficiency in the carbon–carbon and carbon–nitrogen coupling reactions of aryl iodides, bromides and chlorides with olefins and aryl amines was observed in the presence of  $\gamma$ -Fe<sub>2</sub>O<sub>3</sub>@MBD/Pd-Co. Most of the reported methods suffer from lack of generality for the coupling reactions of aryl chlorides. Notably, chloroarenes are the most widely available and inexpensive halides compared with other aromatic halides, but are the most challenging ones. Furthermore, the reported procedures have one or more of drawbacks such as requiring high temperature, large quantity of the catalyst, unrecyclable catalysts, additives and organic solvents. High catalytic performance of Fe<sub>2</sub>O<sub>3</sub>@MBD/Pd-Co is the result of the synergetic cooperative effect of both Pd and Co in  $\gamma$ -Fe<sub>2</sub>O<sub>3</sub>@MBD/Pd-Co and its dispersion in water, due to the encapsulation of MNPs by melamine-based dendrimer, which caused better contact between the catalyst and the reactants. Most importantly, the dispersion of the magnetic catalyst facilitates the catalyst recovery and reuse by ten consecutive extraction and at the end magnetic isolation. Among the reported methods, using water as an ecofriendly solvent, simple catalyst recovery and reuse, easy work-up and not needing any additive make our protocol more environmentally benign method for the C–C and C–N cross-coupling reactions.

## Conclusion

In summary, in this work, melamine-based dendrimer supported on  $\gamma$ -Fe<sub>2</sub>O<sub>3</sub> magnetic nanoparticles was efficiently employed as a suitable material for the in situ preparation of palladium-cobalt nanoparticles by reduction with NaBH<sub>4</sub>. TEM images indicated uniform distribution of fairly small palladium and cobalt alloy nanoparticles supported on the surface of the catalyst. The catalyst was characterized by FT-IR, XRD, XPS, VSM, TGA, ICP and elemental analysis. It was used as a new water-dispersible/magnetically recyclable Pd/Co heterogeneous bimetallic catalyst ( $\gamma$ -Fe<sub>2</sub>O<sub>3</sub>@MBD/Pd-Co) for the efficient Mizoroki–Heck and Buchwald–Hartwig amination reactions in water. A variety of iodo-, bromo- and chloroarenes successfully reacted with acrylates, styrene and anilines to yield the corresponding products. Using this protocol, products were achieved in good to high yields in water as an ecofriendly solvent and without using any additives. The synergistic cooperative effect of both Pd and Co in the encapsulated catalyst leads to high catalytic performance in the cross-coupling reactions in aqueous media. The dispersion of the magnetic catalyst facilitates the catalyst recovery and reuse by ten consecutive extraction and at the end magnetic isolation. The experiments based on isolation of the catalyst in the hot filtration test and using S<sub>8</sub> in the poisoning test, showed that the observed catalysis was heterogeneous in nature. Use of water as an ecofriendly solvent, simple catalyst recovery and reuse, ease of work-up and not needing any additive make this method an environmentally benign procedure for the carbon–carbon and carbon–nitrogen cross-coupling reactions (Supplementary Information).

Entry <sup>[a]</sup>	Aryl halide	Aryl Amine	Product	Time (h)	Isolated Yield (%)
1				4	92
2				4.6	93
3 <sup>[b]</sup>				6.5	89
4				7.3	82
5				3.5	91
6				5.2	89
7 <sup>[c]</sup>				4	90
8 <sup>[c]</sup>				3.5	93
9 <sup>[b, c]</sup>				5.3	88
10 <sup>[c]</sup>				5	85
11 <sup>[c]</sup>				4	90
12 <sup>[c]</sup>				3	95
13 <sup>[c]</sup>				5	90
14 <sup>[c]</sup>				4.2	91
15 <sup>[b, c]</sup>				6	81

**Table 6.** Hartwig–Buchwald amination reaction of assorted haloarenes and arylamines catalyzed by  $\gamma$ -Fe<sub>2</sub>O<sub>3</sub>@MBD/Pd-Co in water. [a] Reaction conditions: aryl halide (1 mmol), arylamines (1.2 mmol), catalyst (0.05 mol% based on the Pd content, except for entries 7–15), and *t*-BuONa (2 mmol, except for entries 3, 9 and 15), 50 °C (except for entries 7–15). The products were characterized by NMR spectroscopy (Figure S14–S18). [b] *t*-BuONa (3 mmol), [c] catalyst (0.07 mol% based on the Pd content), 80 °C.



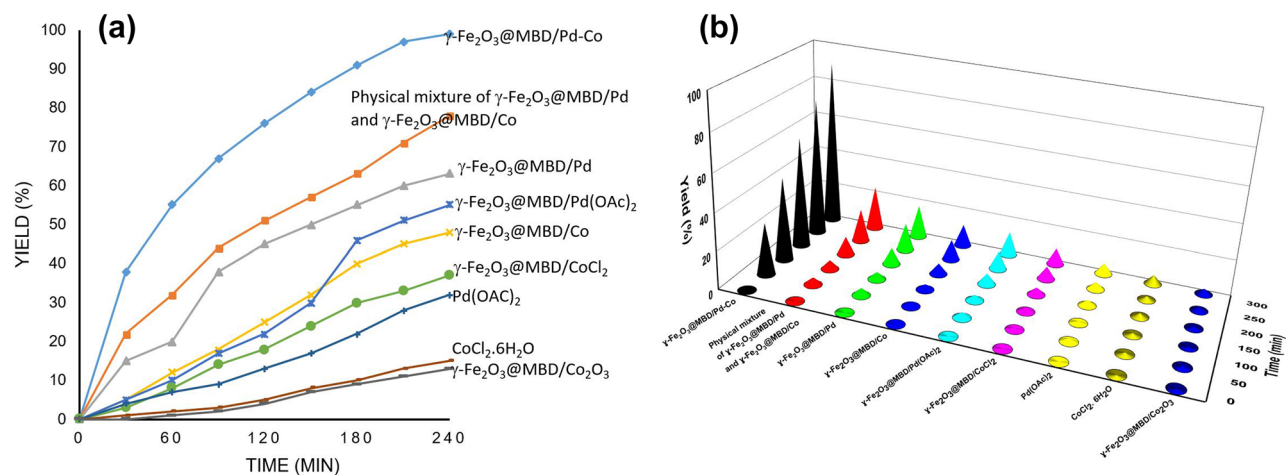
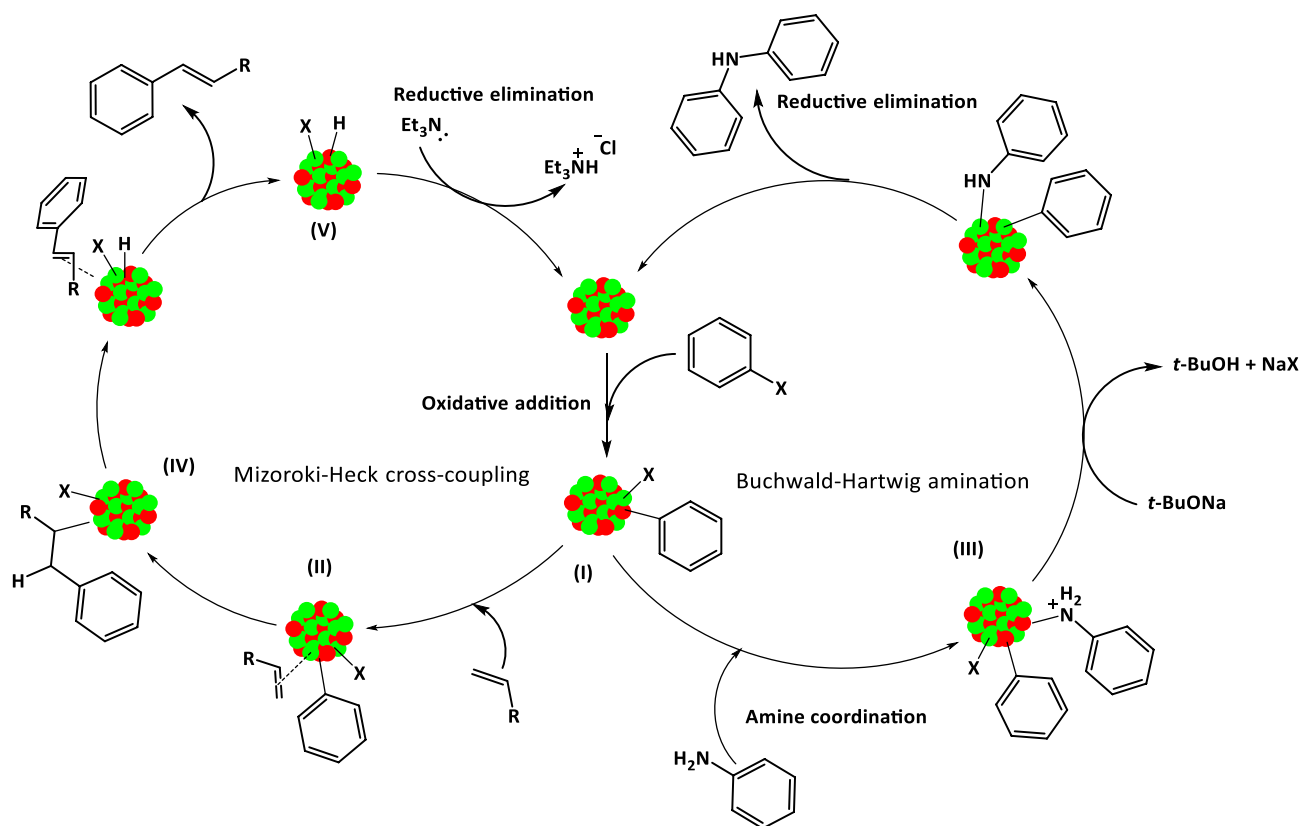


**Figure 12.** Heck and Buchwald–Hartwig amination reactions of chlorobenzene with *n*-butyl acrylate and aniline, respectively, catalyzed by  $\gamma\text{-Fe}_2\text{O}_3\text{@MBD/Pd}$ ,  $\gamma\text{-Fe}_2\text{O}_3\text{@MBD/Co}$ ,  $\text{Fe}_2\text{O}_3\text{@MBD/Pd(OAc)}_2$ ,  $\gamma\text{-Fe}_2\text{O}_3\text{@MBD/CoCl}_2$ , physical mixture of  $\gamma\text{-Fe}_2\text{O}_3\text{@MBD/Pd}$  and  $\gamma\text{-Fe}_2\text{O}_3\text{@MBD/Co}$ ,  $\text{Pd(OAc)}_2$ ,  $\text{CoCl}_2\cdot 6\text{H}_2\text{O}$ , and  $\text{Fe}_2\text{O}_3\text{@MBD/Co}_2\text{O}_3$ ; Reaction conditions: (a) chlorobenzene (1 mmol), *n*-butyl acrylate (1.3 mmol), catalyst (0.05 mol% based on the Pd content or 0.21 mol% based on the Co content),  $\text{Et}_3\text{N}$  (2 mmol), water (1 mL), 50 °C, (b) chlorobenzene (1 mmol), aniline (1.2 mmol), water (1 mL), catalyst (0.07 mol% based on the Pd content or 0.29 mol% based on the Co content), *t*-BuONa (2 mmol), water (1 mL), 80 °C.



**Scheme 2.** Reasonable mechanisms for the Mizoroki–Heck cross-coupling and Buchwald–Hartwig amination reactions.

Entry <sup>ref</sup>	Coupling reaction	Catalyst: amount of Pd (mol %)	Reaction conditions	Ar-X	Time (h)	Yield (%)
1 <sup>70</sup>	Mizoroki–Heck	Pd <sub>63</sub> Sn <sub>37</sub> /C NPs (0.12)	DMF, Et <sub>3</sub> N, 140 °C	I	6	98
				Br		43–95
				Cl		65
2 <sup>71</sup>	Mizoroki–Heck	AuPd/Ni–Al–O (0.2)	DMF, K <sub>2</sub> CO <sub>3</sub> , 100 °C	I	8	92
3 <sup>54</sup>	Mizoroki–Heck	AuPd/ <i>Euphorbia condylocarpa</i> M.bieb NPs(0.2)	H <sub>2</sub> O, K <sub>2</sub> CO <sub>3</sub> , 80 °C, CTAB	I	8	89–95
5 <sup>72</sup>	Mizoroki–Heck	ZnPd/phenanthroline (1)	DMF, K <sub>3</sub> PO <sub>4</sub> , 120 °C, TEAB	I	24	96
6 <sup>73</sup>	Mizoroki–Heck	Ni <sub>0.95</sub> Pd <sub>0.05</sub> NPs (2)	DMF/H <sub>2</sub> O, K <sub>2</sub> CO <sub>3</sub> , 80 °C	I	9–24	48–76
7 <sup>74</sup>	Mizoroki–Heck	Pd <sub>50</sub> Ni <sub>50</sub> /MWCNTs <sup>a</sup> NPs (0.1)	H <sub>2</sub> O, KOH, 120 °C, TBAB	I	1	99
8 <sup>55</sup>	Mizoroki–Heck	PdNi/CL–HA <sup>b</sup> (0.4)	H <sub>2</sub> O, Bu <sub>3</sub> N, 120 °C, TBAB, N <sub>2</sub>	I	12	100
				Br		96–100
				Cl		28–36
10 <sup>8</sup>	Mizoroki–Heck	PdCu/AOT <sup>c</sup> / <i>iso</i> -octane NPs (0.1)	DMF, Et <sub>3</sub> N, 100 °C	I	18	93–100
				Br		74–97
				Cl		66–85
11 <sup>75</sup>	Mizoroki–Heck	Pd <sub>0.1</sub> Au <sub>0.16</sub> /Fe <sub>3</sub> O <sub>4</sub> @LDH <sup>d</sup> (0.05)	DMF/H <sub>2</sub> O, K <sub>2</sub> CO <sub>3</sub> , 120 °C	I	0.67–2	89–99
				Br	2.5–24	43–98
12 <sup>76</sup>	Mizoroki–Heck	Pd–M(M = Ag, Ni, and Cu)/C NPs (0.3)	Acetonitrile, Et <sub>3</sub> N, 82 °C	I	3	35–62
13 <sup>77</sup>	Mizoroki–Heck	MnPd@Py–2,2′–BPPh COF (0.08)	Acetonitrile, K <sub>2</sub> CO <sub>3</sub> , 80 °C, N <sub>2</sub>	I	24	95
14 <sup>78</sup>	Mizoroki–Heck	Hierarchical Pd–Ni/Ni(OH) <sub>2</sub> (0.02)	TBAA, Et <sub>3</sub> N, 160 °C	I	24	87
15 <sup>11</sup>	Mizoroki–Heck	Pd–Co/CoAl–LDH (0.02)	DMF/H <sub>2</sub> O, K <sub>2</sub> CO <sub>3</sub> , 120–140 °C	I	0.5–1.5	91–100
				Br	4–5	92–93
				Cl	10	64
16 <sup>This work</sup>	Mizoroki–Heck	γ–Fe <sub>2</sub> O <sub>3</sub> @MBD/Pd–Co NPs (0.05)	H <sub>2</sub> O, Et <sub>3</sub> N, 60 °C	I	0.4–1.1	95–99
				Br	1.5–2	95–98
				Cl	4–5	90–99
17 <sup>79</sup>	Buchwald–Hartwig amination	PdAu/C (3)	DMSO, <i>t</i> -BuOK, 100 °C	Cl	12	80–99
18 <sup>67</sup>	Buchwald–Hartwig amination	Pd–Ni/B–NPs (0.45)	K <sub>2</sub> CO <sub>3</sub> , H <sub>2</sub> O, 80 °C	Br	5–8	86–100
				Cl	8	69–100
19 <sup>This work</sup>	Buchwald–Hartwig amination	γ–Fe <sub>2</sub> O <sub>3</sub> @MBD/Pd–Co NPs (0.05–0.07)	<i>t</i> -BuONa, H <sub>2</sub> O, 50–80 °C	I	3.5–7.3	89–93
				Br	3.5–5	88–93
				Cl	4.2–6	81–91

**Table 7.** Comparison of catalytic activities of our catalyst with various reported bimetallic Pd catalysts for Mizoroki–Heck and Buchwald–Hartwig amination reactions. [a] Multi-walled carbon nanotube, [b] humic acids, [c] aerosol-OT, [d] layered double hydroxide.

Received: 4 May 2021; Accepted: 2 August 2021

Published online: 23 August 2021

## References

- Boztepe, C., Künkül, A. & Gürbüz, N. Hydrogel supported vinylimidazole based PEPPSI–Pd–NHC catalysts: The catalytic activities in Heck and Suzuki–Miyaura coupling reactions. *J. Mol. Struct.* **1209**, 127948–127960 (2020).
- Madera, J., Slattery, M., Arman, H. D. & Tonzetich, Z. J. Suzuki–Miyaura coupling catalyzed by a Ni(II) PNP pincer complex: Scope and mechanistic insights. *Inorganica Chim. Acta* **504**, 119457–119464 (2020).
- Kanwal, I. *et al.* Palladium and copper catalyzed Sonogashira cross coupling an excellent methodology for C–C bond formation over 17 years: A review. *Catalysts* **10**, 443–491 (2020).
- Sobhani, S., Hosseini Moghadam, H., Skibsted, J. & Sansano, J. M. A hydrophilic heterogeneous cobalt catalyst for fluoride-free Hiyama, Suzuki, Heck and Hirao cross-coupling reactions in water. *Green Chem.* **22**, 1353–1365 (2020).
- Astruc, D. Introduction: Nanoparticles in catalysis. *Chem. Rev.* **120**, 461–463 (2020).
- Chopra, J., Goswami, A. K. & Baroliya, P. K. An overview of solid supported palladium and nickel catalysts for C–C cross coupling reactions. *Mini-Rev. Org. Chem.* **17**, 589–604 (2020).
- Fan, J. *et al.* Recent progress on rational design of bimetallic Pd based catalysts and their advanced catalysis. *ACS Catal.* **10**, 13560–13583 (2020).
- Heshmatpour, F., Abazari, R. & Balalaie, S. Preparation of monometallic (Pd, Ag) and bimetallic (Pd/Ag, Pd/Ni, Pd/Cu) nanoparticles via reversed micelles and their use in the Heck reaction. *Tetrahedron* **68**, 3001–3011 (2012).
- Bayan, R. & Karak, N. Photo-assisted synthesis of a Pd–Ag@CQD nanohybrid and its catalytic efficiency in promoting the Suzuki–Miyaura cross-coupling reaction under ligand-free and ambient conditions. *ACS Omega* **2**, 8868–8876 (2017).

10. Shaabani, A. & Mahyari, M. PdCo bimetallic nanoparticles supported on PPI-grafted graphene as an efficient catalyst for Sonogashira reactions. *J. Mater. Chem. A* **1**, 9303–9311 (2013).
11. Li, J., Song, Y., Wang, Y. & Zhang, H. Enhanced Heck reaction on flower-like Co (Mg or Ni) Al layered double hydroxide supported ultrafine PdCo alloy nanocluster catalysts: The promotional effect of Co. *Dalton Trans.* **48**, 17741–17751 (2019).
12. Slimani, Y. *et al.* In *Smart Nanocontainers* (eds Nguyen-Tri, P. *et al.*) Ch. 14, *Magnetic nanoparticles based nanocontainers for biomedical application* 229–250 (Elsevier, 2020).
13. Xie, W. & Wang, H. Immobilized polymeric sulfonated ionic liquid on core-shell structured Fe<sub>3</sub>O<sub>4</sub>/SiO<sub>2</sub> composites: A magnetically recyclable catalyst for simultaneous transesterification and esterifications of low-cost oils to biodiesel. *Renew. Energy* **145**, 1709–1719 (2020).
14. Yang, Y., Zhu, W., Shi, B. & Lü, C. Construction of a thermo-responsive polymer brush decorated Fe<sub>3</sub>O<sub>4</sub>@catechol-formaldehyde resin core-shell nanosphere stabilized carbon dots/PdNP nanohybrid and its application as an efficient catalyst. *J. Mater. Chem. A* **8**, 4017–4029 (2020).
15. Baran, T. & Sargin, I. Green synthesis of a palladium nanocatalyst anchored on magnetic lignin-chitosan beads for synthesis of biaryls and aryl halide cyanation. *Int. J. Biol. Macromol.* **155**, 814–822 (2020).
16. Ilunga, A. K. & Meijboom, R. A review of dendrimer-encapsulated metal nanocatalysts applied in the fine chemical transformations. *Catal. Lett.* **149**, 84–99 (2019).
17. Sharahi, F. J. & Shahbazi, A. Melamine-based dendrimer amine-modified magnetic nanoparticles as an efficient Pb (II) adsorbent for wastewater treatment: Adsorption optimization by response surface methodology. *Chemosphere* **189**, 291–300 (2017).
18. Veisi, H., Hamelian, M. & Hemmati, S. Palladium anchored to SBA-15 functionalized with melamine-pyridine groups as a novel and efficient heterogeneous nanocatalyst for Suzuki-Miyaura coupling reactions. *J. Mol. Catal. A: Chem.* **395**, 25–33 (2014).
19. Islam, M. S. & Khan, M. W. Synthesis, characterization and catalytic activity of melamine-based dendrimer encapsulated Pd/Cu bimetallic nanoparticles. *Int. J. Nanopart. Res.* **2**, 1–12 (2019).
20. Sobhani, S., Habibollahi, A. & Zeraatkar, Z. A novel water-dispersible/magnetically recyclable Pd catalyst for C-C cross-coupling reactions in pure water. *Org. Process Res. Dev.* **23**, 1321–1332 (2019).
21. Jahanshahi, R., Khazaei, A., Sobhani, S. & Sansano, J. M. g-C<sub>3</sub>N<sub>4</sub>/γ-Fe<sub>2</sub>O<sub>3</sub>/TiO<sub>2</sub>/Pd: A new magnetically separable photocatalyst for visible-light-driven fluoride-free Hiyama and Suzuki-Miyaura cross-coupling reactions at room temperature. *New J. Chem.* **44**, 11513–11526 (2020).
22. Moghadam, H. H., Sobhani, S. & Sansano, J. M. New nanomagnetic heterogeneous cobalt catalyst for the synthesis of aryl nitriles and biaryls. *ACS Omega* **5**, 18619–18627 (2020).
23. Sobhani, S. & Esmaeilzadeh-Soleimani, S. Immobilized palladium-pyridine complex on γ-Fe<sub>2</sub>O<sub>3</sub> magnetic nanoparticles as a new magnetically recyclable heterogeneous catalyst for Heck, Suzuki and copper-free Sonogashira reactions. *Org. Chem. Res.* **5**, 10–24 (2019).
24. Sobhani, S., Ghasemzadeh, M. S., Honarmand, M. & Zarifi, F. Acetamidine-palladium complex immobilized on γ-Fe<sub>2</sub>O<sub>3</sub> nanoparticles: A novel magnetically separable catalyst for Heck and Suzuki coupling reactions. *RSC Adv.* **4**, 44166–44174 (2014).
25. Sobhani, S. & Zarifi, F. Pd-isatin Schiff base complex immobilized on γ-Fe<sub>2</sub>O<sub>3</sub> as a magnetically recyclable catalyst for the Heck and Suzuki cross-coupling reactions. *Chin. J. Cat.* **36**, 555–563 (2015).
26. Sobhani, S. & Pakdin-Parizi, Z. Palladium-DABCO complex supported on γ-Fe<sub>2</sub>O<sub>3</sub> magnetic nanoparticles: A new catalyst for C-C bond formation via Mizoroki-Heck cross-coupling reaction. *Appl. Catal. A Gen.* **479**, 112–120 (2014).
27. Sobhani, S., Zeraatkar, Z. & Zarifi, F. Pd complex of an NNN pincer ligand supported on γ-Fe<sub>2</sub>O<sub>3</sub>@SiO<sub>2</sub> magnetic nanoparticles: A new catalyst for Heck, Suzuki and Sonogashira coupling reactions. *New J. Chem.* **39**, 7076–7085 (2015).
28. Sobhani, S., Zeraatkar, Z. & Zarifi, F. Correction: Pd complex of an NNN pincer ligand supported on γ-Fe<sub>2</sub>O<sub>3</sub>@SiO<sub>2</sub> magnetic nanoparticles: A new catalyst for Heck, Suzuki and Sonogashira coupling reactions. *New J. Chem.* **40**, 8969–8969 (2016).
29. Wu, Z.-G. & Gao, J.-F. Synthesis of γ-Fe<sub>2</sub>O<sub>3</sub> nanoparticles by homogeneous co-precipitation method. *Micro Nano Lett.* **7**, 533–535 (2012).
30. Feng, Y.-S., Lin, X.-Y., Hao, J. & Xu, H.-J. Pd-Co bimetallic nanoparticles supported on graphene as a highly active catalyst for Suzuki-Miyaura and Sonogashira cross-coupling reactions. *Tetrahedron* **70**, 5249–5253 (2014).
31. Wang, Y. *et al.* Synthesis and electrocatalytic alcohol oxidation performance of Pd-Co bimetallic nanoparticles supported on graphene. *Int. J. Hydrogen Energy* **39**, 1325–1335 (2014).
32. Huang, Z. *et al.* In situ inducing electron-donating and electron-withdrawing groups in carbon nitride by one-step NH<sub>4</sub>Cl assisted route: A strategy for high solar hydrogen production efficiency. *Environ. Int.* **126**, 289–297 (2019).
33. Wang, S. *et al.* Au nanoparticle decorated N-containing polymer spheres: additive-free synthesis and remarkable catalytic behavior for reduction of 4-nitrophenol. *J. Mater. Sci.* **50**, 1323–1332 (2015).
34. Mohtasebi, A., Chowdhury, T., Hsu, L. H. H., Biesinger, M. C. & Kruse, P. Interfacial charge transfer between phenyl-capped aniline tetramer films and iron oxide surfaces. *J. Phys. Chem. C* **120**, 29248–29263 (2016).
35. Guo, M., Li, C. & Yang, Q. Accelerated catalytic activity of Pd NPs supported on amine-rich silica hollow nanospheres for quinoline hydrogenation. *Catal. Sci. Technol.* **7**, 2221–2227 (2017).
36. Ghotbinejad, M. *et al.* SPIONs-bis(NHC)-palladium(II): A novel, powerful and efficient catalyst for Mizoroki-Heck and Suzuki-Miyaura C-C coupling reactions. *J. Mol. Catal. A: Chem.* **385**, 78–84 (2014).
37. Girardon, J. S. *et al.* Cobalt dispersion, reducibility, and surface sites in promoted silica-supported Fischer-Tropsch catalysts. *J. Catal.* **248**, 143–157 (2007).
38. Guzzi, L., Schay, Z., Stefler, G. & Mizukami, F. Bimetallic catalysis: CO hydrogenation over palladium-cobalt catalysts prepared by sol/gel method. *J. Mol. Catal. A Chem.* **141**, 177–185 (1999).
39. Dong, Z., Gao, P., Xiao, Y., Chen, J. & Wang, W. Pd-Co nanoparticles supported on calcined Mg-Fe hydrotalcites for the Suzuki-Miyaura reaction in water with high turnover numbers. *Catalysts* **9**, 1061–1070 (2019).
40. Carlsson, A. F., Bäumer, M., Risse, T. & Freund, H.-J. Surface structure of Co-Pd bimetallic particles supported on Al<sub>2</sub>O<sub>3</sub> thin films studied using infrared reflection absorption spectroscopy of CO. *J. Chem. Phys.* **119**, 10885–10894 (2003).
41. Sarkar, A., Murugan, A. V. & Manthiram, A. Pt-encapsulated Pd-Co nanoalloy electrocatalysts for oxygen reduction reaction in fuel cells. *Langmuir* **26**, 2894–2903 (2010).
42. Matsuo, Y. Ordered alloys in the cobalt-palladium system. *J. Phys. Soc. Jpn.* **32**, 972–978 (1972).
43. Kim, D.-S., Kim, J.-H., Jeong, I.-K., Choi, J. K. & Kim, Y.-T. Phase change of bimetallic PdCo electrocatalysts caused by different heat-treatment temperatures: Effect on oxygen reduction reaction activity. *J. Catal.* **290**, 65–78 (2012).
44. Darbem, M. P., Esteves, H. A., de Oliveira, I. M. & Stefani, H. A. α, β-unsaturated 2-ketoglycosides via Pd-catalyzed carbonylative Heck reaction of 2-iodoglycals. *Eur. J. Org. Chem.* **2020**, 5220–5226 (2020).
45. Shiri, M., Fathollahi-Lahroud, M. & Yasaei, Z. A novel strategy for the synthesis of 6H-chromeno [4, 3-b] quinoline by intramolecular Heck cyclization. *Tetrahedron* **73**, 2501–2503 (2017).
46. Dhungana, R. K., Shrestha, B., Thapa-Magar, R., Basnet, P. & Giri, R. Pd-catalyzed regioselective 1,2-dicarbofunctionalization of unactivated olefins by a Heck reaction/enolate cyclization cascade. *Org. Lett.* **19**, 2154–2157 (2017).
47. De Vries, J. G. The Heck reaction in the production of fine chemicals. *Can. J. Chem.* **79**, 1086–1092 (2001).
48. Biffis, A., Centomo, P., Del Zotto, A. & Zecca, M. Pd metal catalysts for cross-couplings and related reactions in the 21st century: A critical review. *Chem. Rev.* **118**, 2249–2295 (2018).

49. Bhakta, S. & Ghosh, T. Emerging nickel catalysis in Heck reactions: Recent developments. *Adv. Synth. Catal.* **362**, 5257–5274 (2020).
50. Hajipour, A. R., Rezaei, F. & Khorsandi, Z. Pd/Cu-free Heck and Sonogashira cross-coupling reaction by Co nanoparticles immobilized on magnetic chitosan as reusable catalyst. *Green Chem.* **19**, 1353–1361 (2017).
51. Wang, Y. & Zhang, M. Schiff base/CuI as a novel efficient catalyst system for Cu-catalyzed Heck reaction in water. *ChemistrySelect* **4**, 9673–9676 (2019).
52. Li, J., Song, Y., Wang, Y. & Zhang, H. Ultrafine PdCu nanoclusters by ultrasonic-assisted reduction on the LDHs/rGO hybrid with significantly enhanced Heck reactivity. *ACS Appl. Mater. Interfaces* **12**, 50365–50376 (2020).
53. Sun, Y., Zhu, X., Guo, D., Chen, X. & Dai, J. Efficient synthesis of PtPd/Fe<sub>3</sub>O<sub>4</sub> nanoparticles and its magnetic recoverability and stable recyclability for the Heck and Suzuki reactions. *Mater. Res. Express* **4**, 075022–075034 (2017).
54. Nasrollahzadeh, M., Sajadi, S. M., Rostami-Vartooni, A. & Khalaj, M. Journey on greener pathways: Use of *Euphorbia condylocarpa* M. bieb as reductant and stabilizer for green synthesis of Au/Pd bimetallic nanoparticles as reusable catalysts in the Suzuki and Heck coupling reactions in water. *RSC Adv.* **4**, 43477–43484 (2014).
55. Qijie, X., Lei, Z., Wenzhong, S. & Yuanchen, C. Catalytic performances of cross-linking humic acids supported Pd/Ni bimetallic catalyst for Heck reaction. *Polish J. Chem. Technol.* **11**, 22–26 (2009).
56. Li, H., Zhu, Z., Li, H., Li, P. & Zhou, X. Recyclable hollow Pd–Fe nanospheric catalyst for Sonogashira-, Heck-, and Ullmann-type coupling reactions of aryl halide in aqueous media. *J. Colloid Interface Sci.* **349**, 613–619 (2010).
57. Goyal, V. *et al.* Carbon-supported cobalt nanoparticles as catalysts for the selective hydrogenation of nitroarenes to arylamines and pharmaceuticals. *ACS Appl. Nano Mater.* **3**, 11070–11079 (2020).
58. Wu, L., Song, Y., Li, Z., Guo, J. & Yao, X. Copper(II)-catalysed aerobic oxidative coupling of arylamines with hexafluoroisopropanol: An alternative methodology for constructing fluorinated compounds. *Adv. Synth. Catal.* **363**, 268–274 (2021).
59. Hasija, D. C., Ghase, V. D., Rananaware, M. M. & Patil, V. R. Ullmann coupling for low-cost synthesis of anthracene-based polyfluorenes: A photophysical approach. *High Perform. Polym.* **33**, 115–124 (2020).
60. Doddi, A., Peters, M. & Tamm, M. N-heterocyclic carbene adducts of main group elements and their use as ligands in transition metal chemistry. *Chem. Rev.* **119**, 6994–7112 (2019).
61. Hartwig, J. F. Transition metal catalyzed synthesis of arylamines and aryl ethers from aryl halides and triflates: Scope and mechanism. *Angew. Chem. Int. Ed.* **37**, 2046–2067 (1998).
62. Kalampour, N., Nejati, S. & Keshipour, S. Pd nanoparticles/graphene quantum dot supported on chitosan as a new catalyst for the reduction of nitroarenes to arylamines. *J. Iran. Chem. Soc.* **18**, 1243–1250 (2021).
63. Mishra, V., Arya, A. & Chundawat, T. S. High catalytic activity of Pd nanoparticles synthesized from green alga *Chlorella vulgaris* in Buchwald–Hartwig synthesis of N-aryl piperazines. *Curr. Organocatalysis* **7**, 23–33 (2020).
64. Masanori, K., Masayuki, K. & Toshihiko, M. Palladium-catalyzed aromatic amination of aryl bromides with N,N-di-ethylamino-tributyltin. *Chem. Lett.* **12**, 927–928 (1983).
65. Forero-Cortés, P. A. & Haydl, A. M. The 25th anniversary of the Buchwald–Hartwig amination: Development, applications, and outlook. *Org. Process Res. Dev.* **23**, 1478–1483 (2019).
66. Nasrollahzadeh, M., Azarian, A., Ehsani, A. & Zahraei, A. Facile synthesis of Fe@Pd nanowires and their catalytic activity in ligand-free C–N bond formation in water. *Tetrahedron Lett.* **55**, 2813–2817 (2014).
67. Heshmatpour, F. & Abazari, R. Formation of dispersed palladium–nickel bimetallic nanoparticles in microemulsions: Synthesis, characterization, and their use as efficient heterogeneous recyclable catalysts for the amination reactions of aryl chlorides under mild conditions. *RSC Adv.* **4**, 55815–55826 (2014).
68. Tsukada, N., Ohnishi, N., Aono, S. & Takahashi, F. Amination of aryl iodides catalyzed by a palladium–copper complex supported by a chelate-bridging ligand. *Organometallics* **31**, 7336–7338 (2012).
69. Tan, B. Y.-H. & Teo, Y.-C. Efficient cobalt-catalyzed C–N cross-coupling reaction between benzamide and aryl iodide in water. *Org. Biomol. Chem.* **12**, 7478–7481 (2014).
70. Li, Y., Dai, Y. & Tian, X.-K. One-pot synthesis of monodisperse palladium tin nanoparticles with controlled composition and size and its catalytic ability study. *Catal. Lett.* **145**, 1837–1844 (2015).
71. Wang, J., Jia, M. L., Tuya, M. G., Wang, J. & Bao, Z. R. G. T. The performance of Au–Pd/Ni–Al–O for Heck reaction. *Adv. Mater. Res.* **955–959**, 494–497 (2014).
72. Lin, R.-S., Li, M.-R., Liu, Y.-H., Peng, S.-M. & Liu, S.-T. Bimetallic complexes of porphyrinphenanthroline: Preparation and catalytic activities. *Inorganica Chim. Acta* **363**, 3523–3529 (2010).
73. Rai, R. K. *et al.* Access to highly active Ni–Pd bimetallic nanoparticle catalysts for C–C coupling reactions. *Catal. Sci. Technol.* **6**, 5567–5579 (2016).
74. Ohtaka, A. *et al.* Palladium and bimetallic palladium–nickel nanoparticles supported on multiwalled carbon nanotubes: Application to carbon–carbon bond-forming reactions in water. *ChemCatChem* **7**, 1841–1847 (2015).
75. Li, J., Wang, Y., Jiang, S. & Zhang, H. Facile synthesis of magnetic recyclable palladium–gold alloy nanoclusters catalysts PdAu<sub>4</sub>/Fe<sub>3</sub>O<sub>4</sub>@LDH and its catalytic applications in Heck reaction. *J. Organomet. Chem.* **878**, 84–95 (2018).
76. Kim, S.-J., Oh, S.-D., Lee, S. & Choi, S.-H. Radiolytic synthesis of Pd–M (M=Ag, Ni, and Cu)/C catalyst and their use in Suzuki-type and Heck-type reaction. *J. Ind. Eng. Chem.* **14**, 449–456 (2008).
77. Leng, W., Ge, R., Dong, B., Wang, C. & Gao, Y. Bimetallic docked covalent organic frameworks with high catalytic performance towards tandem reactions. *RSC Adv.* **6**, 37403–37406 (2016).
78. Fan, H. *et al.* Controllable synthesis of ultrathin transition-metal hydroxide nanosheets and their extended composite nanostructures for enhanced catalytic activity in the Heck reaction. *Angew. Chem. Int. Ed.* **55**, 2167–2170 (2016).
79. Chen, Z. *et al.* Nano PdAu bimetallic alloy as an effective catalyst for the Buchwald–Hartwig reaction. *Asian J. Chem.* **11**, 351–355 (2016).

## Acknowledgements

Financial support of this project by University of Birjand Research Council and Ministerio de Ciencia e Innovación (PID2019-107268GB-I00) are acknowledged. Access to the TEM, EDS-mapping and XPS facilities of University of Alicante is appreciated.

## Author contributions

H.Z. is a Ph.D. student at University of Birjand. He worked under the supervision of me, S.S. He has done all the experiments including catalyst preparation and the experiments related to the application of the catalyst in the reactions. He has also prepared a draft of the manuscript. J.M.S. from Alicante University helped us to analyze the catalyst. He has also read the manuscript and edited it.

## Competing interests

The authors declare no competing interests.

### Additional information

**Supplementary Information** The online version contains supplementary material available at <https://doi.org/10.1038/s41598-021-95931-6>.

**Correspondence** and requests for materials should be addressed to S.S.

**Reprints and permissions information** is available at [www.nature.com/reprints](http://www.nature.com/reprints).

**Publisher's note** Springer Nature remains neutral with regard to jurisdictional claims in published maps and institutional affiliations.



**Open Access** This article is licensed under a Creative Commons Attribution 4.0 International License, which permits use, sharing, adaptation, distribution and reproduction in any medium or format, as long as you give appropriate credit to the original author(s) and the source, provide a link to the Creative Commons licence, and indicate if changes were made. The images or other third party material in this article are included in the article's Creative Commons licence, unless indicated otherwise in a credit line to the material. If material is not included in the article's Creative Commons licence and your intended use is not permitted by statutory regulation or exceeds the permitted use, you will need to obtain permission directly from the copyright holder. To view a copy of this licence, visit <http://creativecommons.org/licenses/by/4.0/>.

© The Author(s) 2021